The Disk-Halo Transition and the Search for Stellar Streams

Carina Lagerholm

Lund Observatory
Lund University

2010-EXA40

Degree project of 60 higher education credits (for a degree of Master)
June 2010

Lund Observatory
Box 43
SE-221 00 Lund
Sweden

Abstract

Recent work by Nissen & Schuster have found two distinct populations of halo stars with $-1.5 \leq$ [Fe/H] ≤ -0.5. Both populations are kinematically selected to be halo stars. The differences between the two groups are the α -elemental abundances and the [Na/Fe] and [Ni/Fe] ratios. From angular momentum space, we can see that the majority of these stars do not show any extreme kinematic indication that they would be part of a halo stellar stream. From the Hipparcos catalogue we have found roughly 50 stars with the same orbital characteristics. Out of these 31 stars have been observed with HARPS at La Silla in Chile and with FIES at the NOT on La Palma. Abundance analysis has been done on 23 stars. From these we can conclude that the two distinct populations of halo stars found by Nissen & Schuster are present in our sample of halo stars. We investigate the differences in these two populations, according to their orbital characteristics and abundances, both for our sample and the Nissen & Schuster sample. We found that the stars with higher α abundances have tendency to be more similar to the disk of the Milky Way than the stars with lower α abundances, seen in angular momentum space. These high α stars also show $U_{\rm LSR}$ and $W_{\rm LSR}$ similar to what is seen for the disk. From studying our sample of stars and stars found in the literature we find a total of 31 new potential stream stars which have extreme kinematics similar to two known stellar streams. We will here present our results from the abundance analysis of these 23 halo stars and a kinematical study of new potential stream stars.

Populärvetenskaplig beskrivning

Vår galax Vintergatan består utav flera olika delar bland annat en disk där större delen utav stjärnbildningen sker, men även en stor sfärisk halo bestående till mesta delen utav äldre stjärnor. Det finns flera olika teorier om hur denna halo skulle kunna ha bildats, men en idé är att åtminstone en del utav den har byggds upp utav betydligt mycket mindre galaxer som har fastnat i Vintergatans gravitation och därmed slitits sönder. När en sådan galax slits söder lämnas ett band utav stjärnor i dess bana runt Vintergatan, dessa band kallar vi för strömmar. Genom att studera dessa strömmars egenskaper och banor kan vi få en uppfattning om Vintergatans gravitation och hur dess utsträckning ser ut. Detta kan ge oss information om t.ex. hur mycket mörk materia (osynlig materia som endast växelverkar med synlig materia genom gravitation) det finns i Vintergatan samt hur den är fördelad. Det svåra ligger i att hitta dessa strömmar, särskilt de som bildades för väldigt länge sedan, typiskt mer än åtta miljarder år sedan. De yngre strömmarna syns fortfarande som områden i halon där densiteten av stjärnor är mycket större, medan de äldre strömmarna har hunnit med att blandas med de redan befintliga stjärnorna i halon, samt att de ljusstarkaste stjärnorna i strömmen har hunnit dö. Dessa äldre strömmar finner man istället genom att studera enskilda stjärnors egenskaper, så som positioner i Vintergatan, deras hastigheter i olika riktningar samt vilka grundämnen de består utav och hur mycket det finns utav dessa ämnen. Stjärnor som bildas på samma ställe, t.ex. i en mindre galax, kommer att ha liknande hastigheter och bestå utav liknade sammansättningar utav olika grundämnen. Stjärnor som uppvisar liknande egenskaper kan därmed antas tillhöra samma ström och komma från samma ursprungsgalax.

I detta examensarbete har vi observerat ett antal stjärnor som tillhör halon. Vi tog spektra utav dessa stjärnor för att kunna göra en grundlig studie utav hur mycket och vilka grundämnen stjärnorna består utav. Utav de stjärnor vi har observerat har vi funnit en som uppvisar egenskaper liknande en redan känd ström. Men eftersom våra observerande stjärnor är få i antalet har vi valt att även titta på stjärnor frn tidigare studier. I dessa studier har man gjort grundliga studier i att kartlägga vad stjärnorna består utav, vi valde att även inkludera deras positioner och hastigeter för att se om vi kunde finna fler stjärnor som potentiellt kan tillhöra kända strömmar. Vi fann ytterligare 30 stycken stjärnor som inte tidigare har associerat med att tillhöra en ström men som uppvisar egenskaper liknande två kända strömmar.

Contents

Chapter 1

Introduction

This project aims at the usefulness of using both the kinematics and elemental abundances of stars in order to find stars, which show similar properties and are part of the same population. In this chapter we introduce the theory used in this project and the results of previous studies found in the literature. In Chapter 2 we will discuss the largest part of the project, the observations, data reduction, and analysis of the sample of halo stars used. The results from both the elemental abundances analysis and the study of kinematics are in Chapter 3.

1.1 The components of the Milky Way

Our galaxy, the Milky Way, is a spiral galaxy with a disk, a bulge and a large halo. Most of the bright stars are located in the disk and the bulge. The disk is the largest of the two components with a radius of $\sim$ 25 kpc and a thickness of $\sim$ 0.6 kpc. The bulge has a radius of $\sim$ 1 kpc. The halo is by far the largest component in the Milky Way with a radius of $\sim$ 50 kpc. The halo contains an old population of stars, so-called population II stars, which have random orbits around the center of the Galaxy.

From the rotational velocity of stars in the disk, such as the Sun, the mass of the Milky Way can be determined, ($M \sim 10^{11} - 10^{12} \mathrm{M}_{\odot}$). This is far greater than the mass of the stars in galaxy, which implies that there is one more component of the Milky Way, the so-called dark matter halo. The mass of the dark matter halo corresponds to roughly 90% of the mass of the Milky Way.

In this project we study stars which show kinematics similar to the halo, however some of them show abundances which are similar to disk stars. We will therefore go into more detail on the structure of the halo and the disk

of the Milky Way.

1.1.1 The Halo of the Milky Way

A little more than a decade ago the general understanding of galaxy halos was that they consist of a smoothly distributed population of stars. This was deduced, e.g., from observations of RR Lyrae stars and globular clusters distributed around the Milky Way (e.g., Wetterer and McGraw, 1996). However, all-sky-surveys such as Hipparcos (Perryman and ESA, 1997) and SDSS (Slone Digital Sky Survey) (York et al., 2000) have changed this picture, uncovering structures in the halo such as lumps and streams of stars. These discoveries changed our view of the formation of galaxy halos. The halos are natural outcomes from an hierarchical formation where parts of the halos are built from accretion of smaller galaxies, e.g., dwarf galaxies (Johnston et al., 2008). These small galaxies, which have been tidally disrupted and accreted by the Milky Way, will leave a trail of stars, i.e., a stellar stream.

Simulations by Johnston et al. (2008) show that a Milky Way type galaxy within a ΛCDM universe will have roughly 10% of its halo stars associated with substructures and streams, which is consistent with what is seen in the Milky Way and Andromeda. The brightest of these streams will be more metal-rich than the halo stars distributed in the smooth halo component. The simulations also show that these substructures seen in the halos of the Milky Way and Andromeda are sensitive to recent, last 8 Gyr, merging events. The substructures will be more prominent in the outer parts of the halo; whereas the inner halo will be relatively smooth.

One of the largest and most profound streams found in the Milky Way is the Sagittarius stream which originates from the Sagittarius dwarf Spheroidal (dSph) galaxy. This stream can be traced almost around the whole Milky Way and it has two bright obvious trails on the north Galactic cap, where one is thought to be a full orbit behind the other.

It is not just small galaxies such as dSph galaxies which leave this type of streams in the halo; globular clusters will do the same if they have eccentric orbits around the Milky Way. These clusters can, due to tidal heating and tidal stripping, be completely disrupted on a timescale of a Hubble time (Gnedin and Ostriker, 1997). This will lead to a situation where many of the globular clusters once seen in the Milky Way would have been disrupted leaving numerous streams in the halo. Palomar 5 is one example of such a globular cluster that has a stream. The Palomar 5 stream is one of the many streams found with the SDSS and covers roughly 20° on the sky (e.g., Odenkirchen et al., 2001, 2009). It has tails both in front and behind the cluster. It is believed that Palomar 5 is in its final stages of total disruption

and has lost 90% of its initial mass (Koch et al., 2004).

Not all streams are as large as the Sagittarius and Palomar 5 streams. Some are not even visible on the sky, since they only consist of a few known stars scattered all over the sky. For example, it is easier to find the recently formed streams in sky surveys such as SDSS, since these streams still consist of large numbers of young and bright stars. Older accretion events are not as bright since the brightest stars have died. These old accretion events have also had time to be more spatially mixed with the other stars in the halo.

To find these smaller, less bright, streams one can make use of the stellar kinematics, i.e. its velocity and angular momentum. How this is done is described in more details in Section 1.2.2. We will also later in this thesis use this technique in order to investigate whether any of our observed halo stars have kinematics similar to two known streams, Section 3.2.

1.1.2 The Disks of the Milky Way

The spiral arms of the Milky Way are gas-rich regions in the disk where the star formation takes place and will therefore have a high density of young bright stars. In our galaxy we can distinguish where these arms are from the distribution of HII regions in the disk. Even today the complexity of the spiral structure is not fully known (see, e.g., Hou et al., 2009).

The disk of the Milky Way is often divided into two components, the thick and the thin disk. The disk of the Milky Way was first divided into two components when it was found that the vertical stellar density profile, derived from the star counts, had to be fitted by two exponentials and not with a single exponential (Gilmore et al., 1989). Later these two disks have also been evident from, e.g., stellar spectroscopy surveys. These studies show different abundance trends for the two disks, and that the thick disk contains an older population of stars than the thin disk (Gilmore et al., 1989). Some possible formation scenarios for the thick disk are e.g.; A violent dynamical heating of the early thin disk caused by satellite accretion, or direct accretion of thick disk material (Gilmore et al., 1989).

A new idea is that the thick disk would arise from radial migration within the early disk, causing the stars to move outward while the gas sinks into the disk. This would enable further star formation to occur in a thin region giving a thin disk with a younger population of stars (Schönrich and Binney, 2009a). In this scenario, the thick stars thus originate in the inner disk with more vigorous star formation and thus their high alpha-abundances can be explained (Schönrich and Binney, 2009a). This theoretical model can also explain the differences in the abundances of the thin and thick disks, but also the similarities such as the overlap in metallicities.

1.2 Hunting for Stellar Streams

There are different ways of finding stellar streams. The latest young accretion events will still be present as brighter regions, streams, on the sky, or as overdensities in position and velocity space. For the stars which were accreted further back in the history of the galaxy, this is not possible. Here we can instead make use of the stars individual angular momenta and find stars which show similar angular momenta.

One other way is to make use of the fact that different populations of stars will show different elemental abundances. Stars which have formed in different regions will show differences in the elemental abundances, i.e. accreted stars will have different abundances than stars which are part of the smooth population of the halo. In this Section we will introduce these different methods further and give some examples of what has been found in previous studies using these methods.

1.2.1 Overdensities of Stars in position and radial velocity

During the last two decades many surveys have been made in order to categorize and map the solar neighborhood, e.g. Hipparcos, SDSS, and RAVE (Radial Velocity Experiment), and in the future Gaia.

Hipparcos measured the velocities and positions of the stars in the solar neighborhood. The Hipparcos catalogue, out to a distance of 125 pc, has been used to find stars which form clusters in position and velocity space (e.g., Chereul et al., 1999).These clusters of stars could be associated with known clusters such as the Hyades and Pleiades, but they also found clusters which were not known at the time, such as Boötes.

An all-sky map can be used not only to find the streams, but also to map the orbits of these streams, which can be used to constrain the galactic potential of the Milky Way. Belokurov et al. (2006) used the SDSS to map the Sagittarius stream, Figure 1.1, when it passes by the Galactic cap and returns to the Galactic plane. They could see two branches of the stream which correspond to material which has been torn off at different times. However, the stars in these two trails show very similar properties such as metallicities, velocities, and densities of stars (Yanny et al., 2009). This can be explained if the two trails were stripped from the Sagittarius dSph galaxy at roughly the same, but slightly separated, times, i.e. no elemental enrichment of the stars have had time to occur in between the stripping events. There is also evidence for an even more distant structure behind one of these branches. They also saw a number of sibling streams which were at the time unknown.

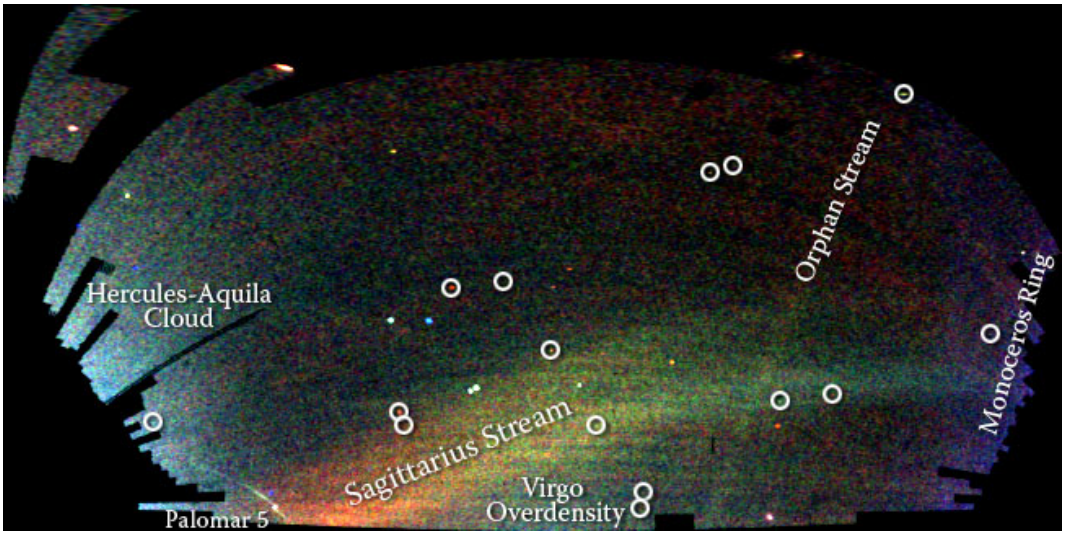

Figure 1.1: The SDSS field of streams constructed from individual red horizontal branch stars, where the red is the most distant stars and the blue the closest. On the y-axis is declination (0-60) and on the x-axis right ascension (220-120). Credit: V. Belokurov and the SDSS.

One of these streams is the Orphan stream, Figure 1.1. The progenitor of the Orphan stream was unknown at the time, hence the name. Fellhauer et al. (2007) showed, by numerical simulations, that the evolution and disruption of the dwarf galaxy Ursa Major II could reproduce the observed data of the Orphan steam, which is now thought to be its progenitor.

It is also possible to use the radial velocities of individual stars to find substructures. Both CORAVEL (Correlation Radial Velocities) and RAVE data have been used to find if there are any stars in the solar neighborhood which are members of large tidal streams (Seabroke et al., 2008), such as the Sagittarius stream. Their sample of stars showed that there are no such streams, containing hundreds of stars, in the close vicinity of the Sun. This also suggests that the Sagittarius stream does not pass through the solar neighborhood, which also agrees with the determinations of its orbit (Chereul et al., 1999), i.e. the Sagittarius, or any other large streams, are all located further away from the Sun.

1.2.2 Angular Momentum Space

The stellar streams seen in sky surveys (which only give the positions of the stars), e.g SDSS, consist of stars which have not yet been spatially mixed with

the smooth population of stars in the halo. These structures are relatively young, but the stars in them may be old. If we instead would like to see further back into the accretion history of the Galactic halo, we need to find stars which have been spatially mixed. These stars are possible to study since they are not mixed in angular momentum and velocity space. The angular momenta are intrinsically stable over a stars whole lifetime (Morrison et al., 2009), meaning that the stars will have the same angular momentum as they had in their accreted progenitor galaxy. This means that stars from the same small accreted galaxy will have similar angular momenta, that differ from those of the normal halo or disk stars.

For the calculation of angular momentum we use the same notation as in Kepley et al. (2007), where a more detailed explanation can be found. The space velocities in the Local Standard of Rest (LSR) are:

$$v_{\rm x} = U + u_{\odot} \tag{1.1}$$
$$v_{\rm y} = V + v_{\odot} + v_{\rm LSR} \tag{1.2}$$
$$v_{\rm z} = W + w_{\odot} \tag{1.3}$$

where U, V and W are the space velocities directed towards the Galactic anti-center, toward the direction of rotation, and towards the north Galactic Pole. $U_{\rm LSR} = v_{\rm x}$, $V_{\rm LSR} = v_{\rm y} + v_{\rm LSR}$ and $W_{\rm LSR} = v_{\rm z}$, where $v_{\rm LSR} = 220$ km s^{-1}. $u_{\odot}$, $v_{\odot}$ and $z_{\odot}$ are the velocity of the Sun relative to the LSR. In this study we use the same values as in Kepley et al. (2007), $[u_{\odot}, v_{\odot}, w_{\odot}] = [-9.0, 12.0, 7.0]$ km s^{-1}.

The angular momentum components are given by the cross products,

$$J_{\rm x} = y v_{\rm z} - v_{\rm y} z \tag{1.4}$$
$$J_{\rm y} = z v_{\rm x} - v_{\rm z} x \tag{1.5}$$
$$J_{\rm z} = x v_{\rm y} - v_{\rm x} y \tag{1.6}$$

The angular momentum space, $J_{\rm plane} = (J_{\rm x}^2 + J_{\rm y}^2)^{1/2}$ vs. $J_{\rm z}$, is shown in both Figure 1.2 and 1.3. All the stars considered here are located in the close vicinity of the Sun (Figure 1.2, Hipparcos catalouge out to ~ 125 pc, with radial velocities and with errors smaller than 10%, taken from the literature), therefore they will have a position in x close to $8kpc$, which means that $J_{\rm z}$ is most sensitive to the rotational velocity, $v_{\rm y}$, in the disk and $J_{\rm plane}$ is sensitive to $v_{\rm z}$, i.e. the velocity perpendicular to the disk.

Stars belonging to the disk of the Milky Way will be located near $J_{\rm z} = 1760$ kpc km s^{-1} due to the rotation velocity in $v_{\rm y}$, Figure 1.2. Halo stars which belong to the smooth component of the halo are located near $J_{\rm z} = 0$ kpc km s^{-1}, this is seen in Figure 1.3.

Several studies have analyzed stellar data in angular momentum space, we have already mentioned Seabroke et al. (2008). Here we will briefly introduce the studies by Helmi et al. (1999), Kepley et al. (2007) and Morrison et al. (2009).

Helmi et al. (1999) found a number of halo stars which are on prograde, high-inclination orbit. These stars are distributed all over the sky and show no spatial structure. The stars are seen as a clump in the angular momentum space, Figure 1.2. Helmi et al. (1999) also made numerical simulations of satellite dispersion in the galactic potential in order to find the properties of the progenitor of these stars. They found that with an evolution of 10 Gyr, the remnants of a dSph galaxy, similar to Fornax, with an initially eccentric orbit and a relatively large apocenter, would be consistent with their positions in angular momentum space.

The stream found by Helmi et al. (1999) was confirmed by Kepley et al. (2007), and they determined that it would have originated from a progenitor galaxy which was accreted between 6 and 9 Gyr ago. They also found two more possible substructures; one retrograde and one prograde group of stars. The prograde group is not as likely to be part of a stream as the retrograde group of stars since it is found in a region of the angular momentum space also occupied by smooth halo stars. The angular momentum of the retrograde group of stars is shown in Figure 1.2. In a study, by Morrison et al. (2009), of RR Lyrae, red giant and red horizontal branch stars located within 2.5 kpc of the Sun, the existence of these two halo streams have been confirmed, Figure 1.3.

1.2.3 Velocity Space

A more simplistic way to find streams is to use the stellar velocities and look directly for stream signatures. However, this method also has its problems, especially in the halo where we might expect the accretion events to have happened some time ago, and thus the stream signatures would be lost. In the disk, however, the possibilities are larger and dynamical structures such as the Hercules moving group is routinely studied in, e.g., the $U - V$ plane (e.g., Bensby et al., 2007). Another tool is the so called Toomre diagram which relates the total non-rotational velocity to the rotational velocity. The Toomre diagram plots the $(U_{\rm LSR}^2 + W_{\rm LSR}^2)^{1/2}$ as a function of $V_{\rm LSR}$. Figure 1.4 shows an example of the general kinematical differences between the halo and the thick and thin disk stars. The main difference between the angular momentum space plots and the Toomre plots are that stars with large $v_{\rm w}$ velocities will end up at high $J_{\rm plane}$ values, meanwhile in the Toomre diagram both stars with either large $v_{\rm u}$ and $v_{\rm w}$ velocities will have high $(v_{\rm x}^2 + v_{\rm z}^2)^{1/2}$

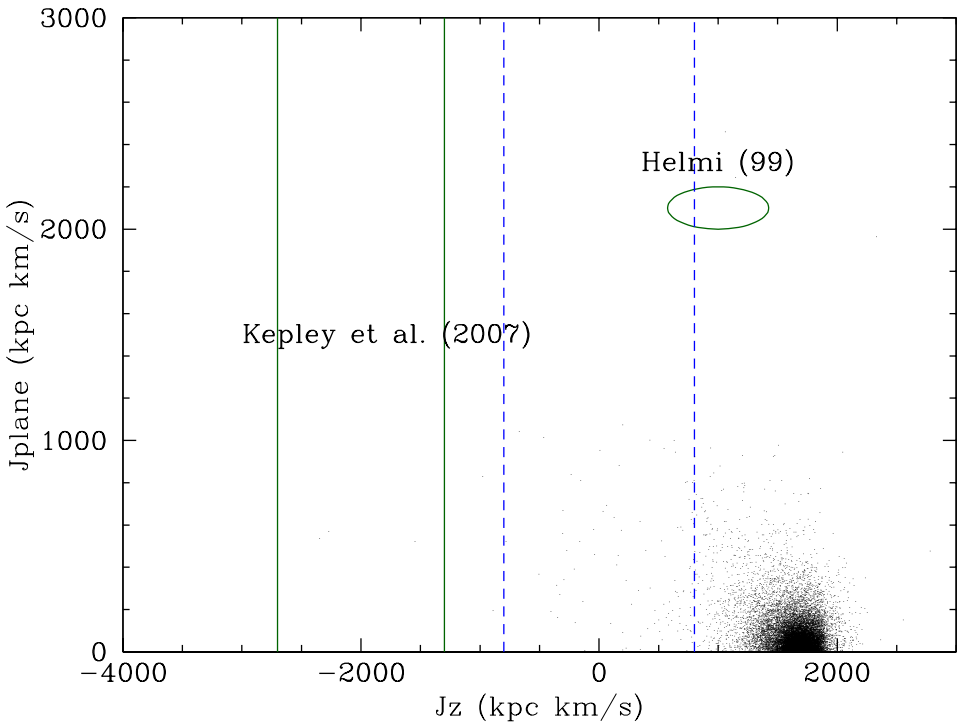

Figure 1.2: Angular momentum plot for stars in the solar neighborhood. The black small dots are stars from the Hipparcos catalogue with radial velocities from the literature. Stars in between the blue dashed lines are likely halo stars. The green ellipse indicates where the stars in the Helmi et al. (1999) stream are located. The stars in the stream found by Kepley et al. (2007) were found in between the green lines.

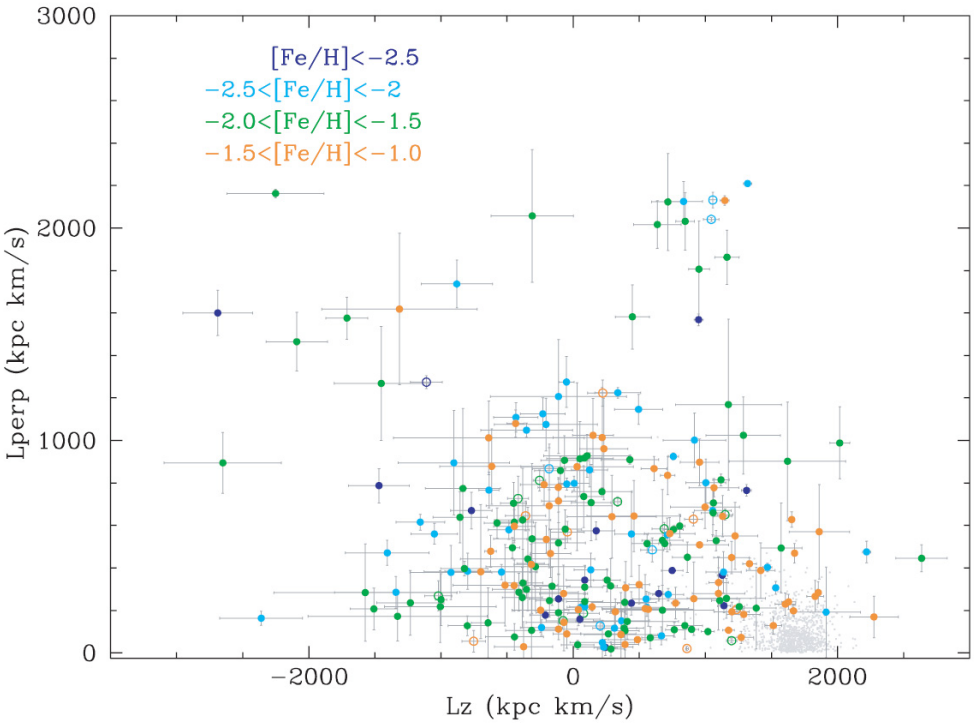

Figure 1.3: From Morrison et al. (2009), the angular momenta J_z vs. J_{plane} for a sample of RR Lyrae stars, red giants and red horizontal branch stars. Colour coded according to the [Fe/H], open circles are red horizontal branch stars. Disk stars from Nordström et al. (2004), with [Fe/H] > -1.0, are shown in gray.

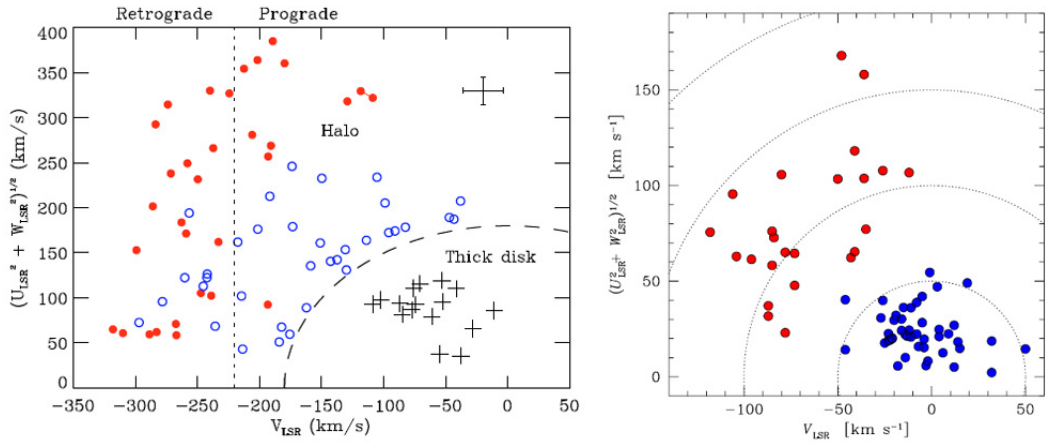

Figure 1.4: Toomre diagram. To the left, thick disk stars (black crosses) and halo stars, high α (blue open circles) and low α (filled red circles), from Nissen and Schuster (2010). To the right, thin (filled blue circles) and thick (filled red circles) disk stars from Bensby et al. (2004).

values. This is discussed more in Section 3.2.2.

1.2.4 Elemental Abundances

The kind of substructures discussed in the previous sections are now also becoming apparent in metallicity and abundance distribution patterns of halo stars. The elemental abundances have an advantage over velocity since they will always be conserved in dwarf stars and not change, unlike velocities that may get disturbed due to interaction with the Milky Way. The differences in the abundance pattens of the α-elements[1] and of iron in accreted stars, is a direct feature that depends on the time of the merger and the mass of the merging galaxy. Therefore, the patterns will be different for each substructure (Johnston et al., 2008, and references therein).

Nissen and Schuster (1997), and in their more recent study Nissen and Schuster (2010), have showed that halo stars with [Fe/H]≥ -1.5 separates into two distinct populations according to their abundances. These stars are kinematically chosen to be halo stars by simply demanding that $V_{\rm tot} \geq$ 180km/s. They also used Strömgren photometry to select only dwarf and subgiant stars. The two halo populations are especially separated in the α-

[1] α-elements are associated with the elements O, Mg, Si, Ca and Ti, which all possess isotopes that are multiples of the α particle, hence the name

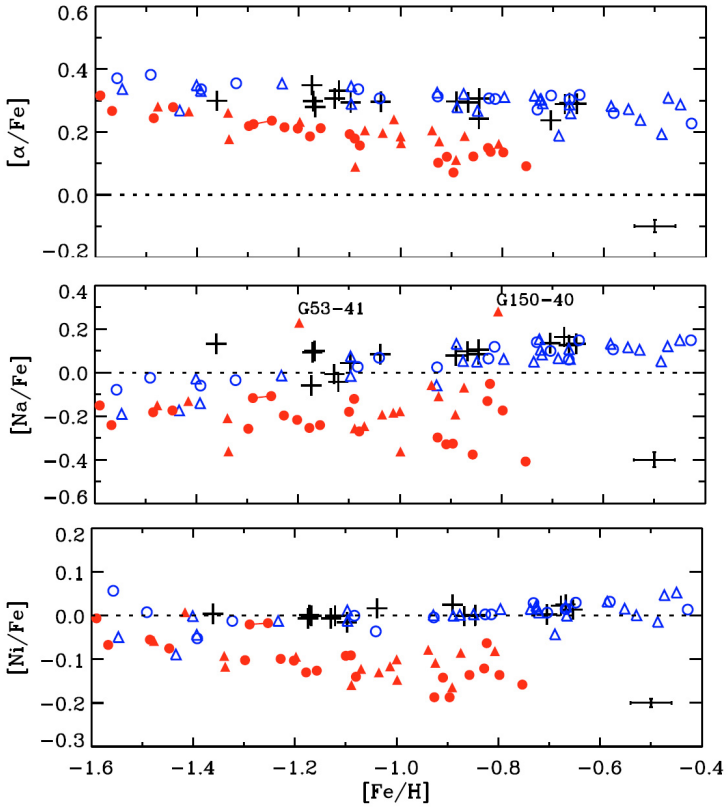

Figure 1.5: From Nissen and Schuster (2010). [α/Fe], [Na/Fe] and [Ni/Fe] as a function of [Fe/H]. The black crosses indicate the disk stars. The blue open circles and triangles are the halo stars with high α-abundances, the red filled circles and triangles are the halo stars with low α-abundances.

elements but also in Ni and Na, Figure 1.5. The population referred to as the high-α stars shows a flat abundance trend similar to that seen for disk stars with similar iron abundances, $-1.5 \leq$ [Fe/H] ≤ -0.5. Meanwhile the low-α population of stars show decreasing α-abundances as [Fe/H] increases. They also show lower abundances of Ni and Na.

The elemental abundances of these two populations indicate that the stars would have formed in at least two different regions, with different star formation rates. The high α-stars were formed in a region with a high star formation rate, were the only contribution to the enrichment of the interstellar medium would come from type II Supernovae. The low-α stars would originate in a region with a lower star formation rate, making enrichment from type Ia Supernovae possible. Type Ia Supernovae enrich the inter-

stellar medium with iron, causing a decrease in [α/Fe] abundances towards higher metallicities. One possibility is that the stars with low α-abundances could be remnants of an accreted galaxy (Nissen and Schuster, 1997).

For lower metallicities, $-2.1 \leq$ [Fe/H] ≤ -1.9, Ivans et al. (2003) found three stars (HIP40068, HIP12710 and CS 22966-043) with low α-element abundances. These stars also show lower abundances of neutron-capture elements, Sr and Ba. The Ni and Na abundances are not lowered as for low-α stars at the higher metallicities in the Nissen and Schuster (2010) sample. By modeling different types of combinations of Supernovae models the α-abundances of the three stars in Ivans et al. (2003) could be explained by a larger contribution of type Ia Supernovae than for the average halo star. These three stars might even have been formed from the material polluted by the first type Ia Supernovae events in the Milky Way. Two of the stars, HIP12710 and CS 22966-043, show high abundances of Ti, Cr, Mn, Ni and Cu. However, these abundances could not be modeled using only type Ia Supernovae (Ivans et al., 2003).

For even lower iron abundances, $-4 \leq$ [Fe/H] ≤ -2, there is a more tight trend in the Mg and Ca abundances. No significant spread or separation can be seen for Mg and Ca as is the case for higher metallicities (Arnone et al., 2005). In the Arnone et al. (2005) sample of turn-off stars the slopes for the linear fit of the Mg and Ca abundances differs. Mg show an almost flat trend towards higher metallicities, while Ca decreases at higher metallicities. This would indicate that Mg and Ca are produced by type II Supernovae with different mass progenitors (Arnone et al., 2005).

1.3 The Future - Combining kinematics, elemental abundances and models

The best thing would be to combine both the kinematics and abundances of stars in order to find stellar streams, but also make use of stellar halo models to better understand the accretion history of the Milky Way. Stellar halo models constructed in standard ΛCDM cosmology have shown that the recent merging history ($0 - 8$Gyr ago) is sensitive to coordinate-space, e.g., as overdensities of stars in SDSS. Meanwhile, the earlier merging history can be seen in the abundance patterns in halo stars, e.g., halos dominated by early accretion have on average higher [α/Fe] ratio than halos dominated by later accretion (Johnston et al., 2008). These models of the stellar halo have also shown that halos, which are dominated by high-luminosity satellites have higher [Fe/H] (Johnston et al., 2008). This can be explained by the

differences in the enrichment timescales of e.g. the α-elements and iron. The α-elements are mostly produced in massive stars which have a short lifetime. Meanwhile, iron is primarily produced in Supernovae type Ia with a much longer timescale. This results in the enrichment of iron being delayed relative to the α-elements. Hence, e.g., halos containing a lot of material accreted early on would have a higher [α/Fe] ratio.

In this thesis we will make use of both the kinematics and the elemental abundance in order to be able to distinguish if any of our observed halo stars could be part of any known stream such as the streams found by Helmi et al. (1999) or Kelpey et al. (2007). Since our sample is small, we will also use the Nissen and Schuster (2010) sample of halo stars, the Schuster catalouge (2006) and the Bensby et al. (in prep.) sample of disk, and halo stars to see if we can find potential stream stars in these (see Section 3.3.1 and 3.3.2).

Chapter 2

Observation and Data Reduction

2.1 Selection of Stars

Nissen and Schuster (1997) showed that halo stars, defined to have $V_{\rm tot} \geq$ 180 km s^{-1}, split into two distinct populations in [α/Fe] for stars with $-1.5 \leq$[Fe/H] ≤ -0.5. The halo stars which showed low α-abundances also showed low [Na/Fe] and [Ni/Fe]. Helmi et al. (1999) showed that it is possible to find substructures in the halo, which are visible in angular momentum space. Therefore we investigated if the stars with low Ni and Na abundances from Nissen and Schuster (1997) shared similar kinematics in angular momentum space. All these stars have a $J_{\rm z} \sim 0$kpc km s^{-1}, which makes them kinematically part of the halo.

We want to investigate if we see the same split in [α/Fe] for similar [Fe/H] as Nissen and Schuster (1997). For this we used a completely kinematically based selection and used the stars' angular momenta to select the sample. To do this we used the Hipparcos catalogue of parallaxes combined with radial velocities from the literature to find stars for which the U, V and W velocities could be calculated. Only stars with parallax errors smaller than 25 % were included. The targets were selected based on a Gaussian distribution centered at $J_{\rm z} = 0$kpc km s^{-1}, with $\sigma = 400$kpc km s^{-1} and we initially included all stars within 2σ. Approximately 50 stars were found, most of these are dwarf stars which are preferred for abundance analysis. We observed 31 of these stars and these are listed in Table 2.1.

2.2 Observations

The observations were made during three different observing runs; two at the Nordic Optical Telescope (NOT) on La Palma and one at La Silla in Chile. In total we had eight nights at the NOT, four in July 2008 and four more in November, Figure 2.2. This first run was done by Jennifer Simmerer and me, the second run by Daniel Adén and me. Due to bad weather in November, with thick fog during the last two nights, only two and a half nights were used for observations. In March 2009 I observed for seven nights at the 3.6 metre telescope at La Silla, see Figure 2.3.

At the NOT we used FIES (FIber feed Echelle Spectrograph) which has a wavelength coverage of 3650 to 7300 Å and a maximum resolution of $67,000$. At La Silla we used HARPS (High Accuracy Radial velocity Planet Searcher), which is also an echelle spectrograph, with a wavelength coverage of 3780 to 6910 Å and a resolution of $120,000$.

A total of 31 stars were observed both in the Northern and Southern hemispheres. Table 2.1 lists the observed stars with their right ascension (RA) and declination (Dec), visual magnitude (V) and spectral type [1].

On each night, calibration frames were taken both before and after the observations. These calibrations consist of bias, flat-field images and Thorium-Argon (ThAr) spectra. We also observed a number of rapidly rotating B-stars during each observing night. This type of star has very few lines and the few visible lines will be broadened due to the high rotation. These stars are used to identify the telluric lines in the spectra of the science targets.

The signal to noise ratios (S/N) for most of the stars are as high as 400. We aimed at this high S/N to be able to measure the forbidden oxygen line at 6300 Å. Unfortunately, it seems that most of the observed stars are too metal-poor for this line to be visible, Figure 2.1 shows an example. Table 2.2 lists the number of exposures taken for each star, the total exposure time, and the S/N. It also lists when and where the observations were carried out.

2.3 Data Reduction

Both the FIES and HARPS spectrographs are structurally isolated from the telescope dome and thermally isolated from the outside world. This means that the instruments are extremely stable which allows for precise and non complicated measurements.

[1] The spectral classes for the observed stars in Table 2.1 are taken from SIMBAD.

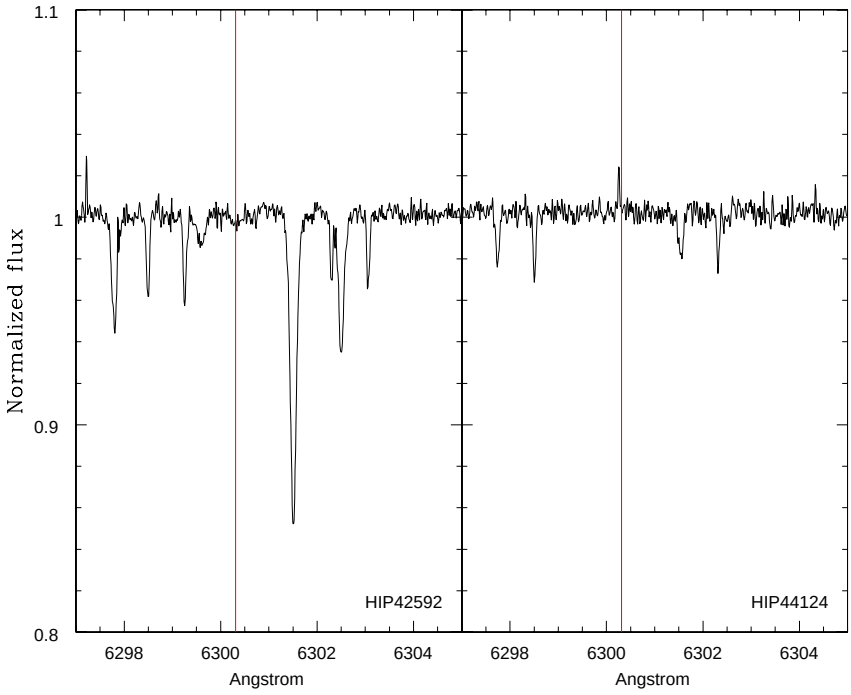

Figure 2.1: Spectra of the two stars HIP42592 and HIP44124 in the region where the oxygen line would be. The position of the oxygen line is indicated with the red line.

Table 2.1: Column one lists the names of the observed stars, column two and three the RA and Dec. Column four lists the visual magnitude and column five the spectral types of the stars (taken from SIMBAD).

Star name	Alt. name	RA	Dec	V [Mag]	Sp. type
HIP3026	HD3567	00 38 31.9465	-08 18 33.400	9.25	F5V
HIP3884	HD4744	00 49 52.7914	+30 27 01.034	7.60	G8IV
HIP5458	HD6833	01 09 52.2645	+54 44 20.274	6.75	G9III
HIP16404	LHS175	03 31 17.3993	+66 43 49.020	9.91	G0
HIP22068	HD30273	04 44 48.6862	-32 52 37.798	9.85	F0V
HIP23344	G 84-29	05 01 16.6219	+04 06 37.021	9.79	sd:F0
HIP28671	HD250792	06 03 14.8623	+19 21 38.676	9.28	G0V
HIP38541	HD64090	07 53 33.1201	+30 36 18.252	8.27	sdG2
HIP42592	HD74000	08 40 50.8039	-16 20 42.522	9.67	sdF6
HIP44124	BD-032525	08 59 10.1122	-04 01 36.518	9.66	F3
HIP48152	HD84937	09 48 56.0984	+13 44 39.320	8.33	sdF5
HIP51477	HD91121	10 30 51.7743	-21 13 37.142	8.73	G1wv...
HIP56327	HD100363	11 32 51.5726	-12 02 06.435	8.64	F2V
HIP56713	HD101063	11 37 40.4027	-28 51 04.849	9.43	K7III
HIP58401	HD104006	11 58 28.0129	-41 55 19.227	8.91	K0.5V
HIP60632	HD108177	12 25 34.9554	+01 17 02.271	9.66	sdF5
HIP62108	HD110621	12 43 43.2206	-44 40 31.559	9.91	F8
HIP63918	HD113679	13 05 52.8241	-38 30 59.996	9.69	G2/G3V
HIP64920	HD115577	13 18 23.4117	-28 19 57.069	6.80	G8IV
HIP65201	HD116064	13 21 43.7934	-39 18 39.918	8.80	sdF0
HIP73385	HD132475	14 59 49.7638	-22 00 45.802	8.55	F5/F6V
HIP76976	HD140283	15 43 03.0966	-10 56 00.590	7.21	sdF3
HIP78640	LHS6300	16 03 13.2990	+42 14 46.645	9.86	F5
HIP80114	HD146296	16 21 11.3153	-71 17 13.018	9.76	G3V
HIP80837	HD148816	16 30 28.4602	+04 10 41.608	7.27	F8V
HIP86694	HD160617	17 42 49.3239	-40 19 15.525	8.72	Fw
HIP94929	HD180928	19 19 00.0965	-15 32 11.651	6.09	K4III
HIP100660	HD229274	20 24 36.0988	+41 30 02.590	9.05	Fp
HIP100792	HD194598	20 26 11.9189	+09 27 00.416	8.33	F7V-VI
HIP103092	HD199191	20 53 18.3147	+54 31 05.168	7.15	GIII+...
HIP103519	HD199870	20 58 19.4647	+44 28 18.158	5.55	K0IIIbCN..

Table 2.2: The number of exposures, total exposure time and resulting S/N ratio for our stars. Column one lists the names of the stars, column two the number of exposures. Column three gives the S/N ratio, column four the total exposure time in minutes, column five and six list the telescope and date on which the observations were preformed.

Star	exp.	Exp. time (min)	S/N	Telescope	Date (MMYY)
HIP3026	6	180	300	NOT	0708
HIP3884	4	120	-	NOT	0708/1108
HIP5458	4	105	-	NOT	0708/1108
HIP16404	16	720	340	NOT	1108
HIP22068	12	360	395	ESO 3.6m	0309
HIP23344	7	315	331	ESO 3.6m	0309
HIP28671	8	360	500	NOT	1108
HIP38541	6	180	430	NOT	1108
HIP42592	8	300	395	ESO 3.6m	0309
HIP44124	4	180	299	ESO 3.6m	0309
HIP48152	4	180	453	ESO 3.6m	0309
HIP51477	3	90	305	ESO 3.6m	0309
HIP56327	4	180	412	ESO 3.6m	0309
HIP56713	10	300	402	ESO 3.6m	0309
HIP58401	4	180	427	ESO 3.6m	0309
HIP60632	6	270	383	ESO 3.6m	0309
HIP62108	4	180	296	ESO 3.6m	0309
HIP63918	8	345	407	ESO 3.6m	0309
HIP64920	2	27	442	ESO 3.6m	0309
HIP65201	3	135	398	ESO 3.6m	0309
HIP73385	7	210	400	NOT	0708
HIP76976	1	30	300	NOT	0708
HIP78640	12	360	400	NOT	0708
HIP80114	9	345	402	ESO 3.6m	0309
HIP80837	2	60	470	NOT	0708
HIP86694	5	165	440	ESO 3.6m	0309
HIP94929	2	14	436	ESO 3.6m	0309
HIP94929	2	25	-	NOT	0708
HIP100660	9	270	470	NOT	0708
HIP100792	4	120	430	NOT	0708
HIP103092	1	60	-	NOT	0708
HIP103519	2	16	-	NOT	0708

Figure 2.2: The Nordic Optical Telescope, July 2008. *Photograph taken by Carina Lagerholm 2008.*

2.3.1 The FIES Data

For the data reduction of the FIES spectra we used FIEStool which is the pipeline designed for the FIES instrument. FIEStool is built on top of existing IRAF tasks from the echelle package and provides a simple GUI to organize the data. It has been constructed for FIES, but it can be used for other echelle spectrographs too. In our case we could use the preset settings in the pipeline. For more information regarding the installation of FIEStools see Appendix A.

Each night is reduced separately, using the combined biases and normalised combined flats, the so called master bias and master flat. In order to find the location of the orders one of the B-stars was used. In total there are 79 orders, where the overlap of the orders is larger in the blue region of the spectra than in the red. For each night one of the ThAr spectra was used to find the wavelength solution; this is done interactively with the **ecindentify** task in IRAF. By assigning some of the lines their actual wavelength (Å), found in the ThAr atlas from the NOT homepage [2], a wavelength solution can be found. In order to get a good wavelength solution a fairly large number of lines need to be assigned their actual wavelength before trying to fit a function/wavelength solution to the ThAr lines. It was very clear when the

[2] www.not.iac.es

Figure 2.3: The ESO 3.6 meter telescope at La Silla, March 2009. *Photograph taken by Carina Lagerholm 2009.*

solution had converged.

By assigning a queue of science frames in FIEStool, the program reduces each frame separately using the correct calibrations. FIEStool subtracts the combined bias frame from the science frame. It also subtracts scattered light, i.e. it makes a 2-D model of the light in the inter-order spaces and subtracts this. FIEStool also divides the science frames by the normalized 2-D flat in order to get rid of pixel-to-pixel variations in the image. The spectra are extracted into individual one-dimensional orders and then corrected for the shape of the blaze. This is done by dividing the extracted spectra with the shape of the blaze derived from the combined flat. The wavelength solution is added to the orders and finally the orders are merged into one long one-dimensional spectrum. Additional information of how FIEStool works and what is done can be found in the User Manual for FIEStool by Eric Stempels which is available on the NOT homepage.

For the spectral analysis we used the individual orders instead of the long one-dimensional spectrum, since it is easier to work with smaller spectral regions and since we do not need to consider what happens to the spectra in the overlapping regions. This was possible since FIEStool saves all the individual steps in the data reduction process in different files.

2.3.2 The HARPS Data

The HARPS data were reduced at the telescope during the observations and therefore no additional data reduction was necessary. The HARPS spectrograph has two CCDs and there is therefore a gap in the middle of the wavelength region at $5304 - 5343.3$ Å.

2.3.3 Fringing in the reduced HARPS spectra

As can be seen in Figure 2.4 there is an anomaly in the continuum for the HARPS spectra. It is seen as a fairly regular wave in the continuum and is seen both in the halo stars and the B-stars. Over such a small wavelength region as a few Å one would expected the continuum to be fairly constant. This effect resembles fringing which is caused by interactions of the incident and reflected light on a CCD. The continuum changes in intensity over an interval of $1 - 2$ Å and is seen in both the blue and red region of the spectra and on both CCDs. We tried two different ways to get rid of the apparent fringing; by finding the periodicity of the pattern and by dividing the stellar spectrum with a B-star spectrum. We describe both procedures in some detail below.

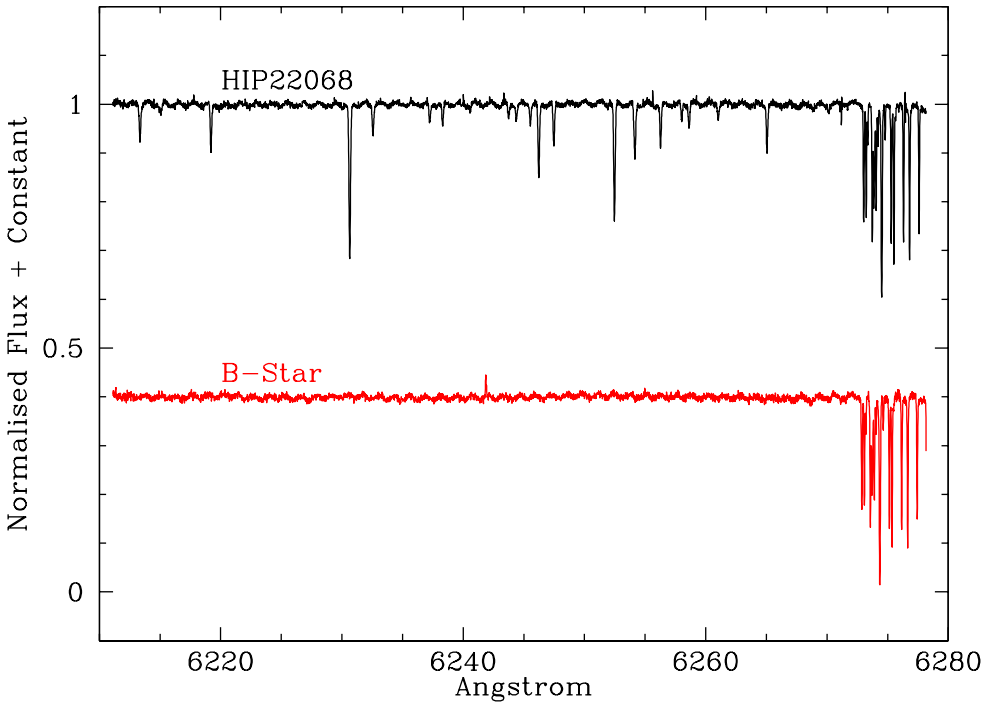

Figure 2.4: The upper black spectrum shows the normalized spectrum of the star HIP22068 without any corrections of the wave pattern. The bottom red spectrum is of a B-star, here the pattern is even more prominent due to the lack of spectral lines.

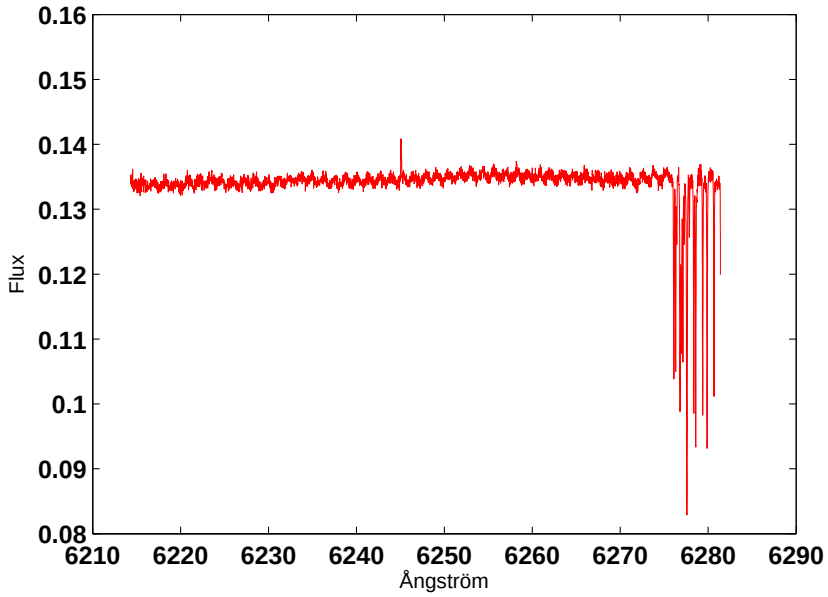

Figure 2.5: The lack of lines makes the fringing more prominent in the rapidly-rotating B-stars. This is the spectrum of the B-star used in the FFT investigation, to see if the fringing is periodic. The only lines visible are the telluric lines at the red side of the spectrum.

Fast Fourier Transform

This small structure in the continuum of the spectra appears, on ocular inspection, to be of a periodic nature[3], therefore an attempt to remove it by Fast Fourier Transform (FFT) was made. To test if this was possible one of the B-stars was used, since these spectra lack spectral features. The spectrum we used is shown in Figure 2.5. The FFT investigation was for simplicity done on a small wavelength region. This is possible since the hypothetical period of the wave pattern is far shorter then the selected wavelength region, Figure 2.6 shows the selected wavelength region. In the power spectrum for this small region one could see just one peak, Figure 2.7. For a larger region, containing spectral lines, more peaks did appear but none of these were more prominent than the others. The small region was therefore favored for further studies. By removing the frequency corresponding to the peak and also the one mirrored in the Nyqvist frequency, the inverse FFT looks a bit better than the original spectrum, as some of the fringing features have disappeared. The result is shown in Figure 2.8.

[3]Pointed out by Ingmar Lundström.

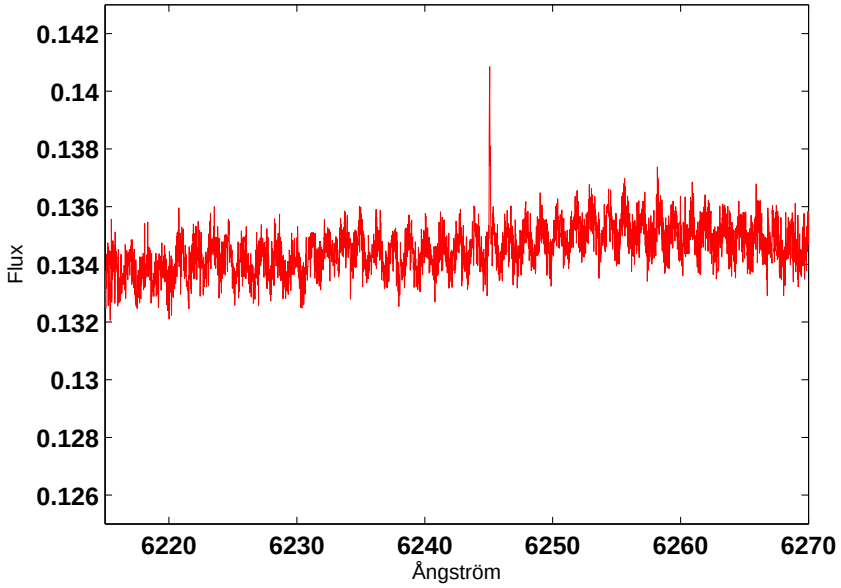

Figure 2.6: The same B-star as in Figure 2.5 but at shorter wavelength range. This is the wavelength range for which the FFT investigation was done.

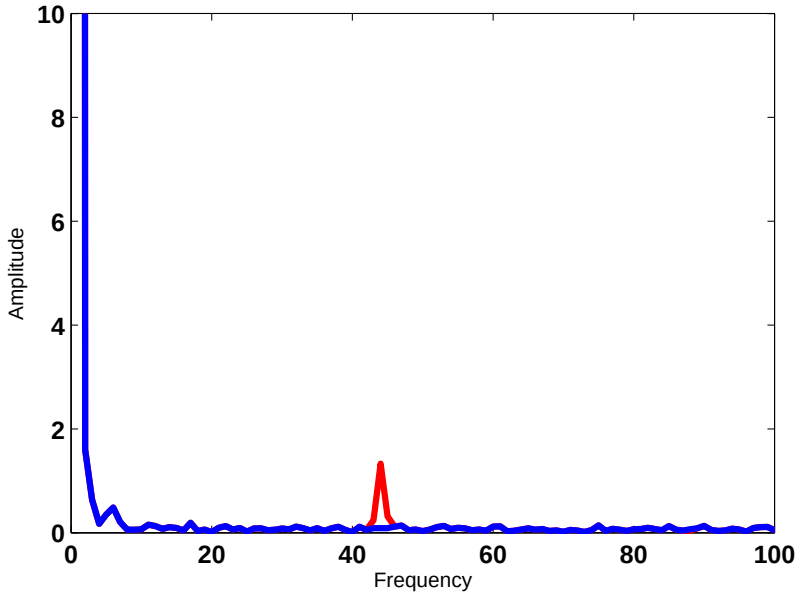

Figure 2.7: The zoomed in power spectrum over the FFT of Figure 2.6. The red peak is the only peak frequency found, this peak was removed, see Figure 2.8.

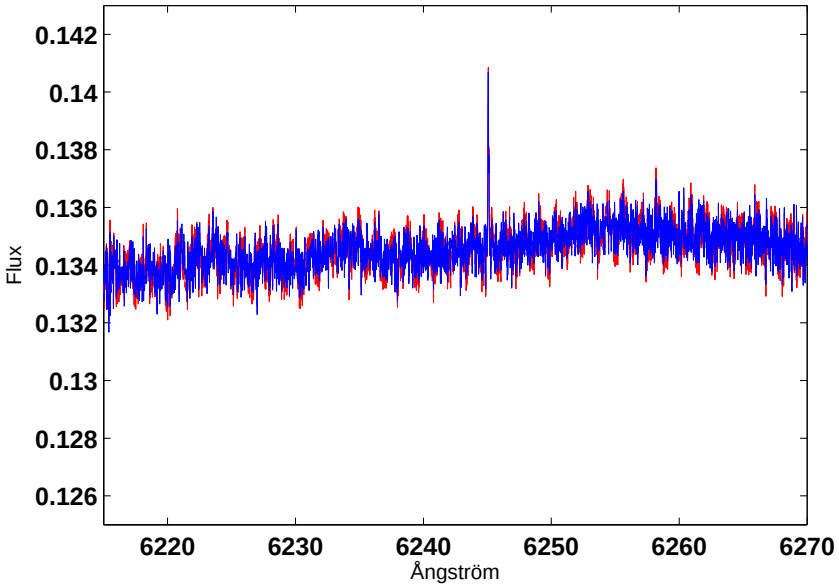

Figure 2.8: The blue spectrum is the inverse FFT of the power spectrum seen in Figure 2.7, the red spectrum is the original B-star spectrum.

The fringing feature has some properties which could indicate that it is made up of one frequency and its overtones. We therefore removed the ten first overtones. The resulting inverse FFT showed that this did not improve the spectrum.

By removing the same peak frequency (Figure 2.7), as seen in the FFT of the small part of the spectra, on the whole order of the B-star spectra and ploting the inverse FFT on top of the original B-star spectrum, one can still see the fringing feature but it has been slightly shifted, shown in Figure 2.9.

From these investigations we conclude that it is not possible to use FFT to clean the spectra (not easily at least) and remove all of the fringing in the continuum[4].

Fast Rotating B-Stars

The fringing feature was instead removed by using the **Telluric** task in **IRAF**, which divides the stellar spectrum with the spectrum from one of the fast rotating B-stars which was observed on the same night as the science frames were taken. The Telluric task takes into account the airmass at

[4]I would like to thank Lennart Lindegren and Melvyn B. Davies for inputs and discussion during the FFT investigation.

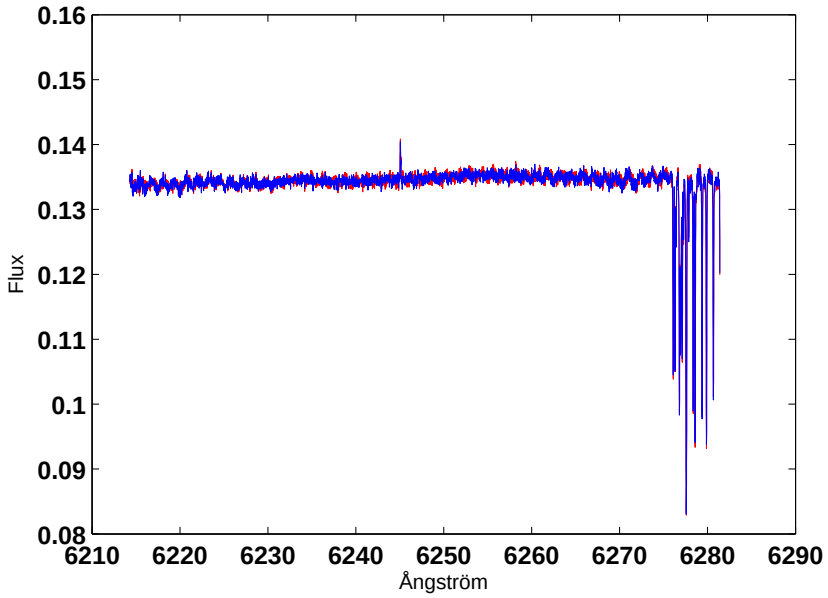

Figure 2.9: The blue spectrum is the same inverse FFT spectrum as in Figure 2.8 but for a larger wavelength region. The red spectrum is the same as in Figure 2.5. It can clearly be seen that the fringing is still visible after removing the peak seen in Figure 2.7, it is smaller in the middle of the wavelength region, but still as prominent as from the beginning in the outer parts.

which the star was observed. Since the telluric lines are located at the same observed wavelength in both the stellar spectra and the B-star spectra, this task does not just remove the fringing in the spectrum but also the telluric lines. The result can be seen in the lower panel in Figure 2.10.

During the reduction of the HAPRS spectra, the spectra are corrected for the shift of the lines due to the rotation of the Earth. These shifts are different for each observation. Therefore it is necessary to shift the spectra before using the Telluric task, otherwise the telluric lines will not be at the same observed wavelength. After the fringing is removed the spectra are shifted back again before all the spectra from one star are compiled into one spectrum to gain S/N.

It is also possible to use the **sarit** task in IRAF for dividing two spectra, but sarit does not take the airmass into account. By testing both methods the telluric was chosen since it gave the highest S/N in the final spectra.

2.3.4 Measuring Equivalent widths

Equivalent widths of the elements and ions Na, Al, Mg, Si, Ca, TiI, TiII, CrI, CrII, FeI, FeII, Ni, Zn, YII and Ba were found by measuring the spectral lines by using the **splot** task in IRAF. The lines which were measured are located from 4500 Å to the end of the spectra, which is at 6800Å for the HARPS spectra and 7300 Å for the FIES spectra. Since the stars are metal-poor it was not possible to measure all the lines in the list given by Thomas Bensby. In the end between 200 and 350 lines were measured for each star depending on the metallicity. The number of lines used in the final abundance analysis for each star are listed in Table B.1 to B.8

2.3.5 Solar Spectra

When performing abundance analysis based on equivalent widths measured in stellar spectra, it is important to also have a solar spectrum for comparison. This solar spectrum needs to be taken during similar circumstances, i.e., using the same instrument. The abundance ratios of the Sun are needed to normalize the stellar abundances to the solar abundances.

In the case of the HARPS spectra, more than one Solar spectrum was taken. Some spectra contained light reflected off the Moon and some of the sky, in both cases the integrated light of the Sun. To add these two types of spectra together you need to take into account the differences in the line shifts due to the different paths of the light. The light from the Moon will have a small shift in the spectra due to the radial velocity of the Moon (around 5km/s in this case), corresponding to the Moons orbital motion, compared

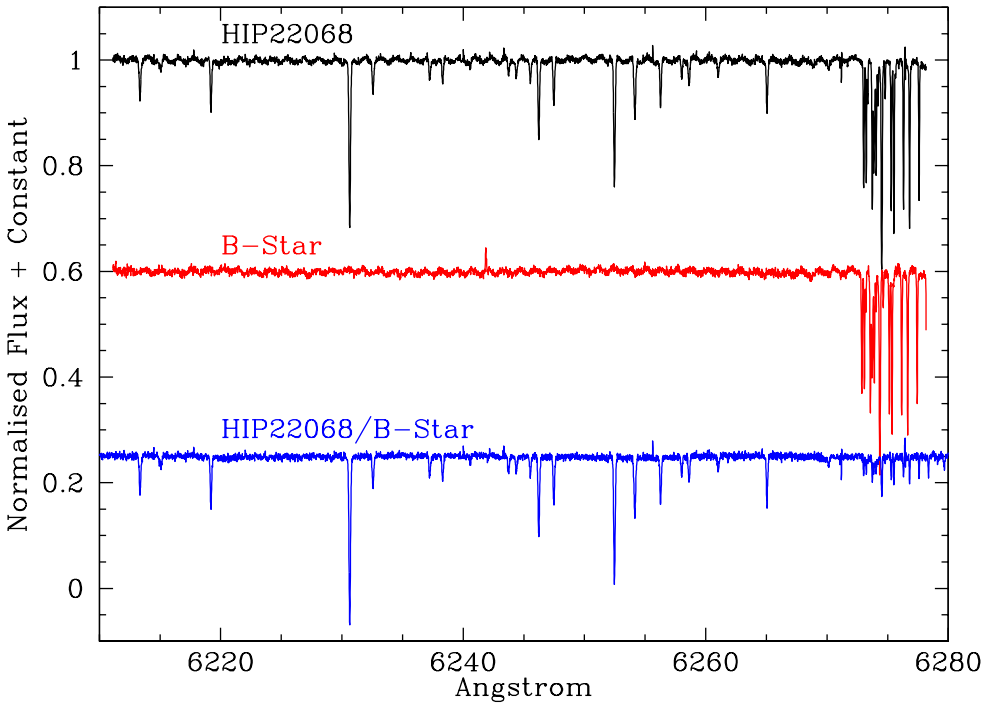

Figure 2.10: The upper, black spectrum shows the spectrum of the star HIP22068 without any corrections. The middle red spectrum is of a B-star, here the apparent fringing is more prominent due to the lack of spectral lines. The bottom spectrum shows the spectrum of the star HIP22068 after it has been corrected for the apparent fringing pattern using the telluric task in IRAF.

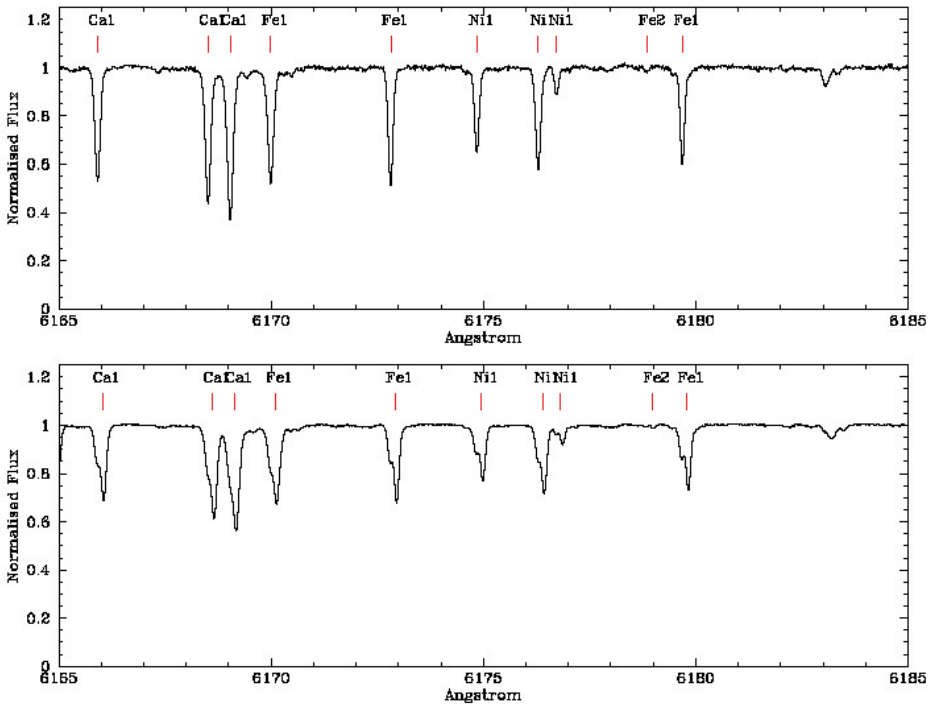

Figure 2.11: The upper spectrum contains just one of the spectra taken of the Moon. The bottom spectrum consists of all the spectra taken of the Moon and the sky. Here you can see how the lines are shifted and broadened compared to the upper spectrum.

to the light reflected from the sky. If you add the Moon and sky spectra together without taking this into account the lines will be broadened. This is shown in the lower panel in Figure 2.11.

For the measurements of the equivalent widths of the Sun we used for simplicity only one of the spectra of the Moon. This particular spectrum, seen in the upper panel in Figure 2.11, has a S/N $\sim$ 500 and is therefore of similar quality as the final, co-added stellar spectra.

2.4 Elemental Abundance Analysis

The abundance analysis was done with the help of Thomas Bensby. We wanted to have a sample which is comparable with his sample of disk stars (Bensby et al. in prep.). Indeed, as we use exactly the same methods our data are directly comparable to his data without any need to consider, e.g.,

systematic offsets.

2.4.1 Selection of Lines

Not all measured lines might be suitable for abundance analysis. Some lines might be affected by unseen blends or telluric lines that have been poorly removed (in the case of the HARPS spectra). For example if a, line in a specific star gives an abundances which deviates a lot from the abundances given by all the Ca lines in this specific star, it will result in an overall abundance of Ca which might be false and have a large error, σ. Some lines might be unsuitable for abundance analysis in a specific star, but suitable in the rest of our sample of stars, this would cause the line to have an offset compared to all other Ca lines and creates an additional random scatter in the abundances trends.

In order to investigate if some lines need to be discarded, we plot the abundances derived from a specific line in a star minus the mean abundances for that specific element and star. An example of Ca is shown in Figure 2.12 where all the individual lines for Ca are plotted for each star in our sample.

A few lines were discarded from all stars since they showed a large scatter around the mean or a large offset from the mean. The lines which were discarded from all the stars are listed in Table 2.3. The three lines which were discarded from the final abundance of Ca are also marked in red in Figure 2.12 a). For a few stars some additional lines were discarded due to their large offsets, Table 2.4.

As an example Table 2.5 shows the differences between the Ca abundances, σ and the number of Ca lines for each star, before and after some lines were discarded from the calculation of the mean abundances for each star. This shows that values of σ are smaller for all the stars in our sample after the removal of the lines with the largest deviations.

2.5 Error analysis

2.5.1 The error in the abundances, σ

The abundance errors, σ, are given by

$$\sigma = \sqrt{\frac{\sum(x_j - \bar{x})^2}{N-1}} \tag{2.1}$$

where x_j is the abundance derived from line j, $\bar{x}$ is the mean abundance for the star and N is the number of lines (Gray, 2005). The error-bars shown

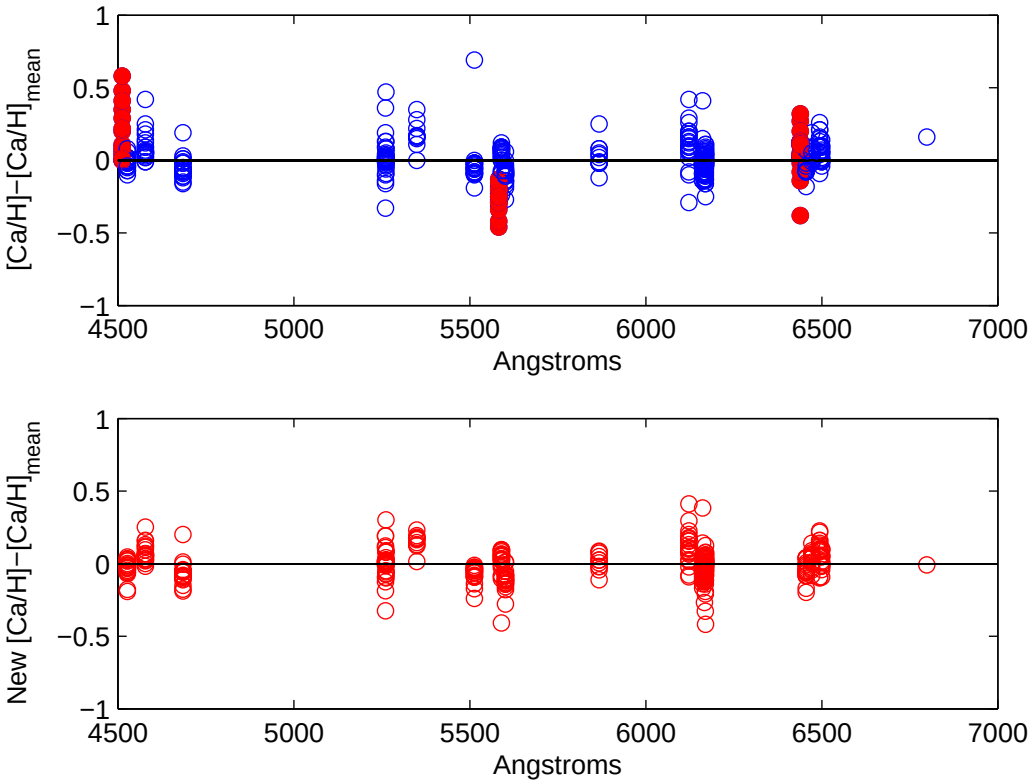

Figure 2.12: The abundances for each specific Ca line and star, minus the mean abundance for Ca for each star. a) All measured lines, where each line in each star is indicated with a open blue circle. The red filled circles indicated the lines which were discarded from all the stars in our sample of halo stars. b) The lines which were kept in each star, normalized to the new mean abundance for each star. The red open circles indicate each specific line and star.

Table 2.3: The lines which were discarded from the abundance analysis for all stars. Column one lists the element, column two the wavelength of the line, column three the atomic number and column four the ion.

Element	λ (Å)	No.	Ion
Si	5665.560	14	I
Ca	4512.270	20	I
Ca	5581.960	20	I
Ca	6439.080	20	I
Ti	4913.610	22	I
Ti	5087.060	22	I
Ti	6743.120	22	I
Ti	4563.760	22	II
Ti	4708.670	22	II
Cr	5783.890	24	I
Cr	5237.330	24	II
Fe	4576.340	26	II
Fe	4635.320	26	II
Ni	4831.170	28	I
Ni	5587.850	28	I
Ni	6643.630	28	I
Y	5402.770	39	II

Table 2.4: The lines which were discarded from the abundance analysis for specific stars. Column one lists the name of the star, column two to six the wavelength for the certain line.

HIP	Si I	Ca I	Ti I	Zn I	YII
3884	5512.980;6122.220				
44124		6161.300			
48152		4526.930	4518.020;4555.480	6362.340	
65201					5662.920
86694	6145.020				

Table 2.5: An example of the differences between the Ca abundances before and after lines were discarded from the abundance analysis. Column one lists the Hipparcos number of the star, column two to four the old [Ca/H], σ and the number of lines used in the abundance analysis. Columns five to seven lists the new [Ca/H], σ and the number of lines used. Columns eight and nine lists the differences between the old and the new [Ca/H] and σ.

HIP	$[Ca/H]_{old}$	$\sigma_{Ca,old}$	$No._{old}$	$[Ca/H]_{new}$	$\sigma_{Ca,new}$	$No._{new}$	Δ [Ca/H]	$\Delta\sigma$
3026	-0.77	0.16	19	-0.79	0.09	16	0.02	0.07
3884	-0.56	0.44	20	-0.39	0.40	15	-0.17	0.04
16404	-1.90	0.15	15	-1.87	0.14	13	-0.03	0.01
22068	-1.06	0.15	20	-1.06	0.14	17	0.00	0.01
28671	-0.73	0.09	21	-0.75	0.08	18	0.02	0.01
38541	-1.40	0.11	22	-1.40	0.08	19	0.00	0.03
42592	-1.56	0.13	18	-1.57	0.11	16	0.01	0.02
44124	-1.39	0.30	16	-1.37	0.10	13	-0.02	0.20
48152	-1.67	0.56	17	-1.62	0.12	14	-0.05	0.02
51477	-0.67	0.09	21	-0.65	0.07	18	-0.02	0.02
58401	-0.44	0.18	21	-0.43	0.14	18	-0.01	0.04
60632	-1.25	0.17	20	-1.25	0.06	17	0.00	0.11
62108	-1.13	0.14	20	-1.13	0.09	17	0.00	0.05
63918	-0.41	0.08	21	-0.41	0.05	18	0.00	0.03
64920	-0.13	0.09	21	-0.14	0.06	18	0.01	0.03
65201	-1.27	0.12	14	-1.28	0.10	12	0.01	0.02
73385	-1.07	0.12	17	-1.04	0.10	15	-0.03	0.02
76967	-2.20	0.18	10	-2.15	0.14	9	-0.05	0.04
78640	-1.01	0.11	18	-1.01	0.10	15	0.00	0.01
80114	-0.46	0.08	21	-0.46	0.06	18	0.00	0.02
80837	-0.46	0.09	20	-0.45	0.07	17	-0.01	0.02
86694	-1.39	0.11	18	-1.36	0.10	16	-0.03	0.01
100792	-0.85	0.12	19	-0.85	0.08	16	0.00	0.04

for all the stars in, e.g., Figure 3.1 $\bar{\sigma}$ is the mean error, which is defined as

$$\bar{\sigma} = \frac{\sigma}{\sqrt{N}} \tag{2.2}$$

The error for [X/Fe] is given by

$$\bar{\sigma}_{[\mathrm{X/Fe}]} = \sqrt{\bar{\sigma}_{\mathrm{X}}^2 + \bar{\sigma}_{\mathrm{Fe}}^2} \tag{2.3}$$

2.5.2 Comparison with other studies

Six of the stars analyzed in this study have also been analyzed by Nissen and Schuster (2010). This means that we can compare these two studies in order to see if there are any systematic differences. The effective temperature, surface gravity and micro turbulence are compared in Table 2.6. The abundances are compared in Table 2.7.

For four of the six stars we have derived a higher effective temperature. We have an estimated error of $\sigma T_{\mathrm{eff}} \pm 70$ K; Nissen and Schuster (2010) have an error of ± 30 K. This means that four of the stars are inside the error margins. It is only HIP73385 which shows a large difference between the two studies. The values for the gravity, log(g), are higher for four of the stars in our analysis than in Nissen and Schuster (2010). Five of the stars show lower values of the micro turbulence, ξ_{turb}, in our analysis and for three of these the differences are quite large especially for HIP63918 where the difference is ~ 0.7 km/s, Table 2.6. The mean of the differences in the micro turbulence could indicate that there is a systematic difference in our study compared to Nissen and Schuster (2010), giving lower ξ_{turb} values, which in turn would imply higher elemental abundances if all the other parameters were the same. However, it appears that our somewhat, in the mean, higher T_{eff} is counteracting this.

Both [Mg/Fe] and [Si/Fe] show lower abundances for the six stars in our study than in Nissen and Schuster (2010). The differences are fairly small and never larger than ~ 0.11 dex, Table 2.7. Both [Cr/Fe] and [Ni/Fe] show a positive mean difference for the six stars, which might indicate systematic differences in the abundance analysis resulting in larger abundance ratios in our sample. For [Fe/H], [Na/Fe], [Ca/Fe] and [Ti/Fe] the differences between our analysis and Nissen and Schuster (2010) do not show any systematic differences. This is also indicated by very small mean differences between our abundances and Nissen and Schuster (2010).

Table 2.6: Comparison between the six stars which are in our sample and in Nissen & Schuster (2010). Columns two to four are from our analysis, columns five to seven are from Nissen & Schuster (2010). Columns eight to ten are the differences between our values and the values from Nissen and Schuster (2010).

ID	$T_{\rm eff}$ (K)	log(g)	$\xi_{\rm turb}$ (km/s)	$T_{\rm eff}$ (K)	log(g)	$\xi_{\rm turb}(km/s)$	$\Delta T_{\rm eff}(K)$	Δlog(g)	$\Delta\xi$ (km/s)
	Our	Our	Our	N&S	N&S	N&S	Our-N&S	Our-N&S	Our-N&S
HIP3026	6153	4.21	1.55	6051	4.02	1.5	102	0.19	0.05
HIP28671	5454	4.24	0.79	5489	4.47	1.1	-35	-0.23	-0.31
HIP63918	5671	4.17	0.70	5672	3.99	1.4	-1	0.18	-0.7
HIP73385	5868	3.90	1.55	5646	3.76	1.5	222	0.14	0.05
HIP80837	5918	4.16	1.15	5823	4.13	1.4	95	0.03	-0.25
HIP100792	5996	4.31	1.25	5942	4.33	1.4	54	-0.02	-0.15
Mean							73	0.05	-0.22

Table 2.7: Comparison between the six stars which are in our sample and in Nissen & Schuster (2010).

ID	$[\frac{Fe}{H}]$	$[\frac{Fe}{H}]_{N\&S}$	$\Delta[\frac{Fe}{H}]$	$[\frac{Na}{Fe}]$	$[\frac{Na}{Fe}]$	$\Delta[\frac{Na}{Fe}]$	$[\frac{Mg}{Fe}]$	$[\frac{Mg}{Fe}]$	$\Delta[\frac{Mg}{Fe}]$	$[\frac{Si}{Fe}]$	$[\frac{Si}{Fe}]$	$\Delta[\frac{Si}{Fe}]$
		N&S		N&S		N&S		N&S				
HIP3026	-1.14	-1.16	0.02	-0.23	-0.24	0.01	0.12	0.14	-0.02	0.11	0.17	-0.06
HIP28671	-1.06	-1.01	-0.05	-0.15	-0.18	0.03	0.12	0.23	-0.11	0.07	0.13	-0.06
HIP63918	-0.68	-0.65	-0.03	0.05	0.15	-0.10	0.28	0.37	-0.07	0.25	0.33	-0.08
HIP73385	-1.41	-1.49	0.08	-0.01	-0.02	0.01	0.40	0.41	-0.01	0.40	0.51	-0.11
HIP80837	-0.70	-0.73	0.03	0.10	0.14	-0.03	0.29	0.32	-0.03	0.20	0.29	-0.09
HIP100792	-1.12	-1.09	-0.03	-0.10	-0.12	0.02	0.17	0.18	-0.01	0.15	0.18	-0.03
Mean			0.003			-0.01			-0.04			-0.07
ID	$[\frac{Ca}{Fe}]$	$[\frac{Ca}{Fe}]_{N\&S}$	$\Delta[\frac{Ca}{Fe}]$	$[\frac{Ti}{Fe}]$	$[\frac{Ti}{Fe}]$	$\Delta[\frac{Ti}{Fe}]$	$[\frac{Cr}{Fe}]$	$[\frac{Cr}{Fe}]$	$\Delta[\frac{Cr}{Fe}]$	$[\frac{Ni}{Fe}]$	$[\frac{Ni}{Fe}]$	$\Delta[\frac{Ni}{Fe}]$
		N&S		N&S		N&S		N&S				
HIP3026	0.37	0.31	0.06	0.23	0.22	0.01	0.04	-0.05	0.09	-0.02	-0.13	0.11
HIP28671	0.33	0.33	0	0.10	0.26	-0.16	0.05	0.04	0.01	-0.13	-0.12	-0.01
HIP63918	0.27	0.32	-0.05	0.25	0.26	-0.01	0.02	0.02	0	0.03	0.03	0
HIP73385	0.34	0.37	-0.03	0.28	0.24	0.04	0.14	-0.03	0.17	0.11	0.01	0.10
HIP80837	0.24	0.25	-0.01	0.21	0.22	-0.01	0.05	0.00	0.05	0.05	0.03	0.02
HIP100792	0.27	0.22	0.05	0.15	0.13	0.02	0.07	-0.04	0.11	-0.02	-0.09	0.07
Mean			0.003			-0.02			0.07			0.05

Chapter 3

Results and Discussion

3.1 Elemental Abundances of 23 Halo Stars

In this section we will begin by discussing the abundances of our sample of 23 halo stars with $-2.5 \leq$[Fe/H]≤ -0.5. We will compare our results with the results from Nissen and Schuster (2010) and also with a sample of disk and some halo stars from Bensby et al. (in prep.).

The elemental abundances for the 23 halo stars analyzed in this study are shown in Figure 3.1.

3.1.1 Introductory notes

The subgiant HIP3884 (red triangle) has a large σ for all the elemental abundances. It also shows large deviations from stars at similar [Fe/H] in this study. Therefore it will be disregarded from further discussion. HIP76976 at [Fe/H] $= -2.57$, also shows large deviations for some of the elements, especially Ni and Ba. Nevertheless we will not disregard it from further discussions since σ is small for most of the elements.

For stars with [Fe/H] ≤ -1.7 the number of lines used for the abundance analysis is reduced by half compared to stars with [Fe/H] ≥ -1.7. The number of lines used for each element and star and the [X/H] abundances and σ are listed in Tables B.1 - B.8 in the Appendix.

3.1.2 Abundances for Mg, Si, Ca, and Ti

The elements Mg, Si, Ca and Ti are also called α-elements, since they are all multiples of the α particle. These elements are formed in the cores of massive stars and introduced into the interstellar medium by type II supernovae.

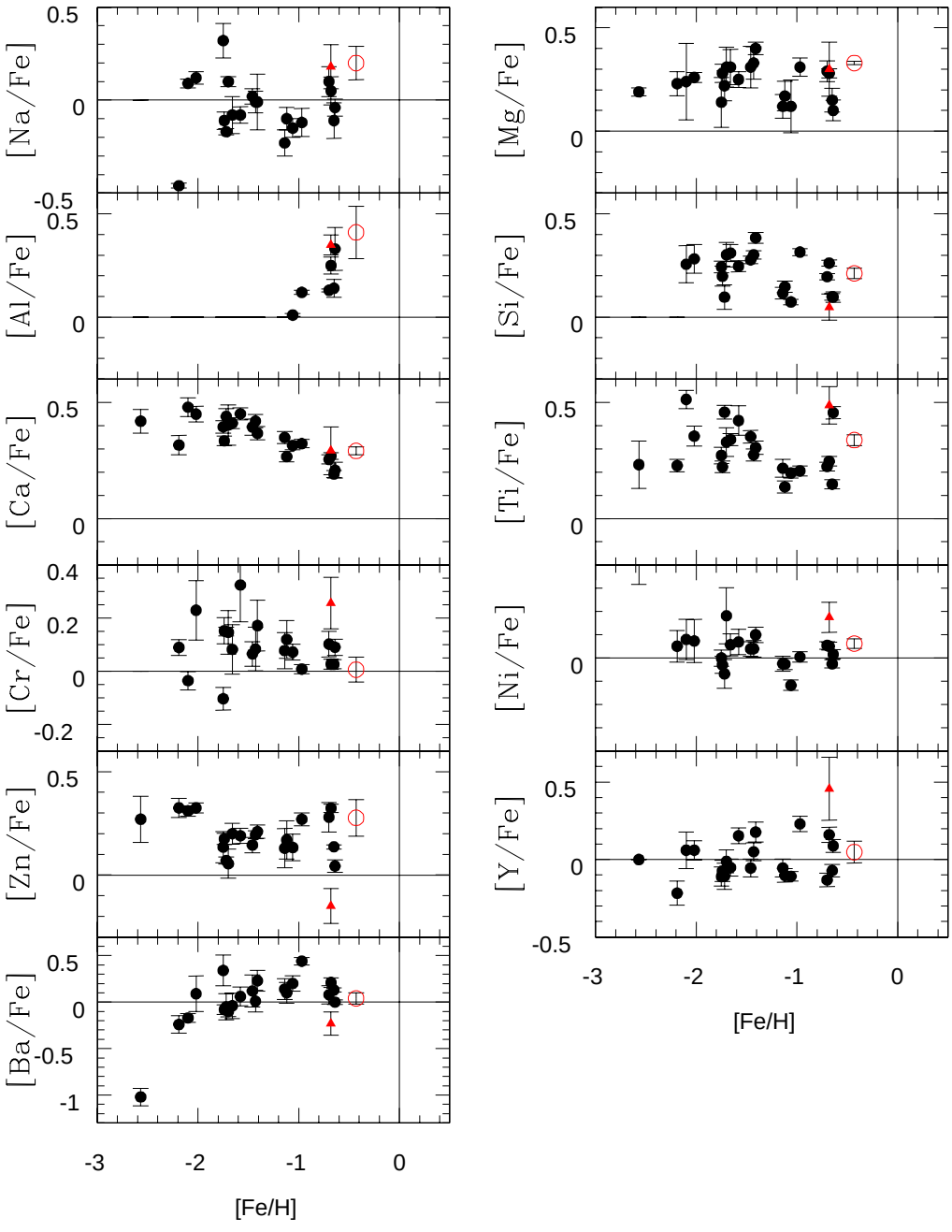

Figure 3.1: Abundances [X/Fe] as a function of [Fe/H] for the 23 halo stars in this study. Dwarf stars are plotted with filled black circles. The two subgiants HIP3884 (filled triangle) and HIP64920 (open circle) are plotted in red.

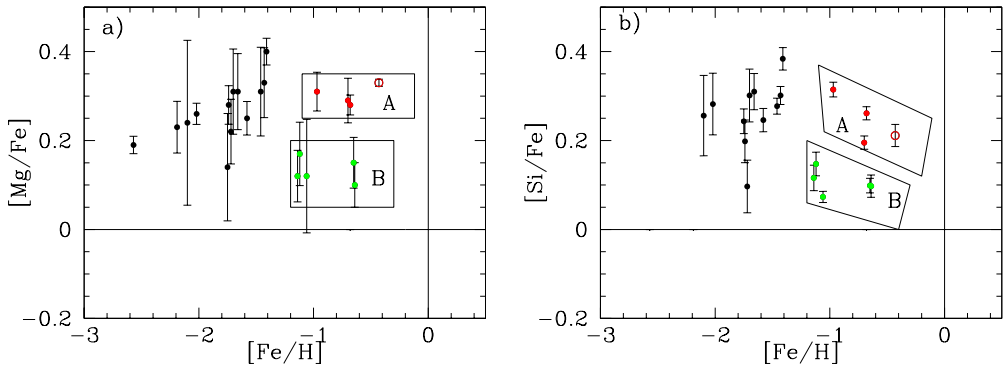

Figure 3.2: Abundances for [Mg/Fe] and [Si/Fe] as a function of [Fe/H]. Filled circles are abundances for dwarf stars and the open circle the subgiant HIP64920. The stars that are part of group A are shown in red and the stars in group B in green. The two groups A and B are highlighted with borders.

The abundances of Mg and Si for our stars are shown in Figure 3.2. Stars with metallicities [Fe/H] > -1.5 split into two groups in [Mg/Fe]. The separation between these two groups is ~ 0.1 dex. In Figure 3.2 these two groups are marked as A (in red) and B (in green). The dwarf stars HIP51477, HIP63918, HIP80837, and the subgiant HIP64920 are members of group A. The five dwarf stars HIP3026, HIP28671, HIP58401, HIP80114, and HIP100792 are members of group B. Throughout the rest of this report we will make use of this division into group A and B. For [Fe/H] ≤ -1.5 no split into separate groups is seen.

The stars show the same type of split in [Si/Fe] as in [Mg/Fe] for stars with [Fe/H] > -1.5. Again the separation between the two groups is ~ 0.1 dex. The stars with higher [Si/Fe] abundances are the same stars which have higher [Mg/Fe] abundances, i.e., the stars in group A show higher abundances in both [Mg/Fe] and [Si/Fe] compared to the stars in group B.

Group A shows a flat trend of [Mg/Fe] and a sloping trend with decreasing abundances of [Si/Fe] towards higher metallicities. For [Fe/H] ≤ -1.5 [Si/Fe] also shows an essentially single trend.

The abundances for Ca and Ti are shown in Figure 3.3. The [Ca/Fe] abundances show a very tight trend for the whole metallicity range. There is no such obvious split for [Fe/H] > -1.5 as seen for both [Mg/Fe] and [Si/Fe]. However, if we mark groups A and B in Figure 3.3 we see that the stars in group A have higher [Ca/Fe] abundances than stars in group B at similar metallicities.

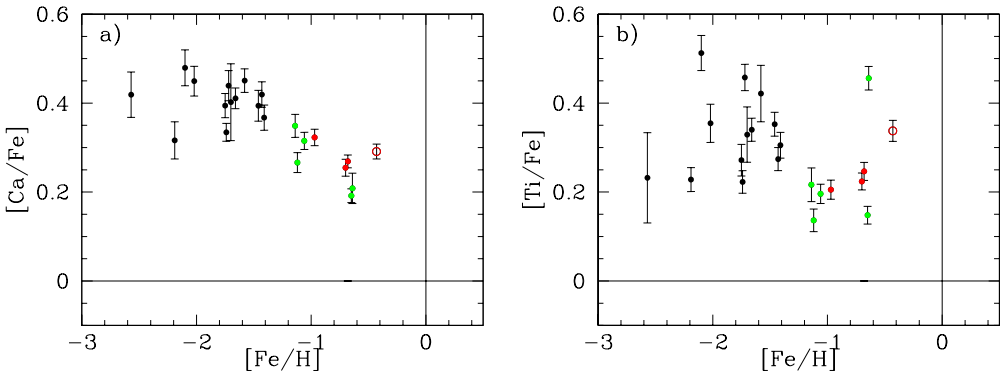

Figure 3.3: Abundances for [Ca/Fe] and [Ti/Fe] as a function of [Fe/H]. The symbols and colours are the same as in Figure 3.2.

The abundances of [Ti/Fe] show a large scatter over the whole metallicity range. The stars in group A and B are less clearly separated than for the other elements.

3.1.3 Na and Ni abundances

The study by Nissen & Schuster (2010) discussed in Section 1.2.4 showed that the [Na/Fe] and [Ni/Fe] abundances in halo stars with $-1.5 \leq$[Fe/H] ≤ -0.5 splits into two groups similar to what we see for [Mg/Fe] and [Si/Fe].

As shown in Figure 3.4 there is a large scatter in the [Na/Fe] abundances for our stars in the whole metallicity range. HIP16404 ([Na/Fe] = −0.46, [Fe/H] = −2.19) shows a much lower [Na/Fe] abundance then the rest of the stars. Three of the stars in group A have higher [Na/Fe] abundances then stars in group B. HIP51477 ([Na/Fe] = −0.12, [Fe/H] = −0.97) has a lower [Na/Fe] abundance then the rest of the stars in group A, which makes it similar to the stars in group B.

The [Ni/Fe] abundances for stars with [Fe/H] > -1.5 show small individual errors. At [Fe/H] ≤ -1.5 the errors in the [Ni/Fe] abundances are larger. This effect might be because only 2-15 lines were used to determine the abundance of Ni for these low [Fe/H] stars, compared to 20-43 lines for stars with [Fe/H] > -1.5.

Stars in group A generally has higher [Ni/Fe] abundances than group B at similar metallicities.

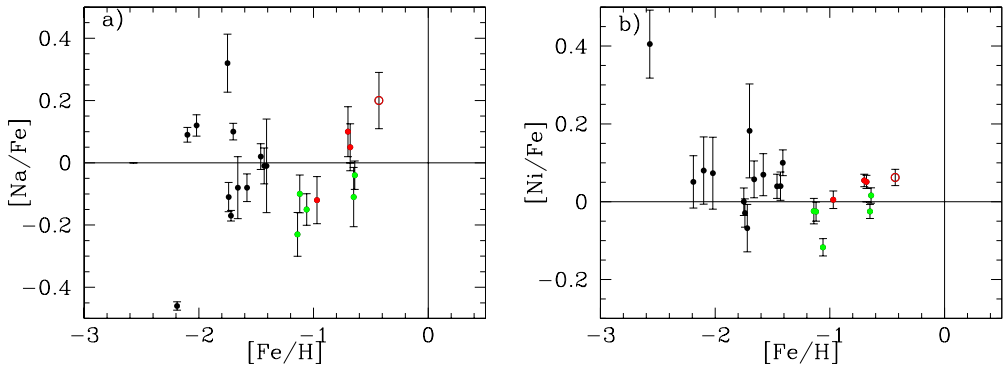

Figure 3.4: Abundances for [Na/Fe] and [Ni/Fe] as a function of [Fe/H]. The symbols and colours are the same as in Figure 3.2.

3.1.4 Y and Ba abundances

Both Y and Ba are s-process (slow neutron capture) elements produced in the He-burning phase in both low and high mass stars.

At [Fe/H] > -1.5 there is a split in the [Y/Fe] abundances for our halo stars. The origin of the split is unknown. We investigated whether the high [Y/Fe] stars with [Fe/H] > -1.5 have, e.g., high $T_{\rm eff}$. We can conclude that the split is not caused by temperature differences between the stars in this metallicity range. On the other hand three of the stars belonging to group A are associated with the higher [Y/Fe] abundances, and four out of five of the stars in group B have lower abundances. The stars with [Fe/H] ≤ -1.5 show no specific trend in [Y/Fe] abundances.

As shown in Figure 3.5 there is no grouping of stars with respect to their [Ba/Fe] abundances. The two groups of stars, A and B, are mixed and no structure is seen. HIP76976 has the most extreme abundance at [Ba/Fe] $= -1.02$ and the reason for this is not clear. Ba is known to have NLTE effects which might explain the scatter of the Ba abundances.

3.1.5 Al abundances

It was only possible to measure Al abundances for eight of the 23 stars in our sample. All of these stars have [Fe/H] ≥ -1.5, Figure 3.6. The abundances of Al for the halo stars in this study are also compared with the Al abundances for disk and halo stars in Bensby et al. (in prep.). Here we use the same classification of the halo and the thick and thin disk used in, e.g., Bensby et al. (2003). The [Al/Fe] abundances for the halo stars are compati-

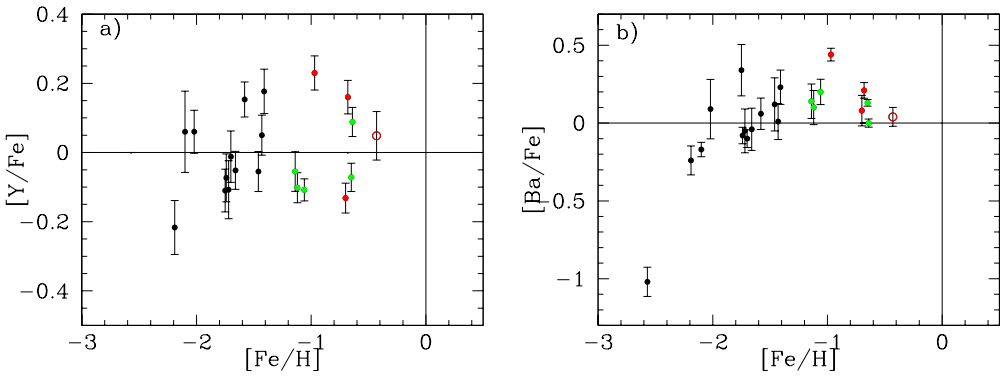

Figure 3.5: Abundances for [Y/Fe] and [Ba/Fe] as a function of [Fe/H]. The symbols and colours are the same as in Figure 3.2.

ble with those found for the disk and the halo stars in Bensby et al. (in prep.).

3.1.6 Iron peak, Cr and Zn abundances

[Cr/Fe] shows a large spread and the individual abundance errors are also large for several of our halo stars. No split in [Cr/Fe] abundance for the two groups of stars, A and B, is seen. The [Cr/Fe] abundances are increasing for several of the stars with decreasing metallicities.

For [Zn/Fe] our halo stars are again split into two groups for [Fe/H] > -1.5. The stars in the two groups are the same stars as in groups A and B, as defined in Section 3.1.2. This means that the [Zn/Fe] abundances show the same type of split as [Mg/Fe] and [Si/Fe] for stars with [Fe/H] > -1.5.

For [Fe/H] ≤ -1.5 the stars divide into two different groups in [Zn/Fe]. One group has $-1.8 \leq$ [Fe/H] ≤ -1.5, these have lower [Zn/Fe] abundances then the group with [Fe/H] ≤ -1.8, which show significantly larger [Zn/Fe] abundances.

3.1.7 Comparison with the Nissen and Schuster sample

We now compare our results with those of Nissen and Schuster (2010). This is done for Mg, Si, Na, and Ni, shown in Figure 3.8 and 3.9. For [Mg/Fe] and [Si/Fe], Figure 3.8, it is clear that our sample of halo stars follows the same abundance trends as the Nissen and Schuster (2010) sample, with similar separation between the two groups of stars for [Fe/H]$\geq$ 1.5. It is also clear

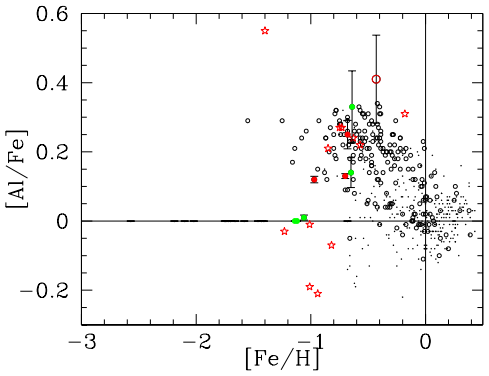

Figure 3.6: Abundances for [Al/Fe] as a function of [Fe/H]. The symbols and colours are the same as in Figure 3.2. The small black dots are thin disk, the open black circles thick disk, and the red open stars are halo stars from Bensby et al. (in prep).

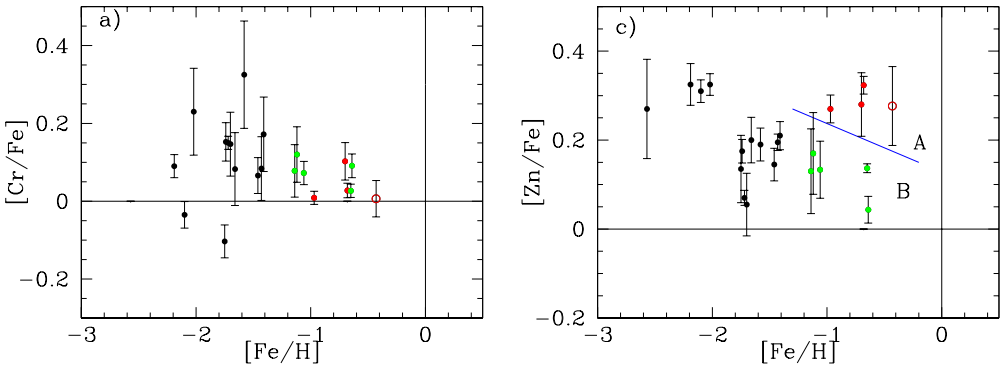

Figure 3.7: Abundances for [Cr/Fe] and [Zn/Fe] as a function of [Fe/H]. The symbols and colours are the same as in Figure 3.2.

Table 3.1: Stellar parameters of the 23 stars presented in this study. Column one lists the name, column two the effective temperature and column three log(g). Column four lists the micro turbulence, column five the mass of the star. Columns six to eight list the estimated age, the upper and lower age.

Star name	$T_{\rm eff}$ (K)	Log(g)	ξ km s^{-1}	Mass ($M_{\odot}$)	Age (Gyr)	Age$_{\rm lower}$ (Gyr)	Age$_{\rm upper}$ (Gyr)
HIP3026	6153	4.21	1.55	0.9	10.2	8.9	11.2
HIP3884	5095	2.98	0.70	1.55	1.8	1.2	2.5
HIP16404	5223	4.55	1.20	0.70	-	-	-
HIP22068	6155	4.01	1.00	0.85	11.2	8.0	12.5
HIP28671	5454	4.24	0.79	0.68	-	-	-
HIP38541	5407	4.57	1.00	0.70	-	-	-
HIP42592	6290	4.21	0.90	0.78	13.3	11.2	15.0
HIP44124	6351	4.64	2.40	0.90	-	-	5.0
HIP48152	6386	4.07	1.90	0.80	12.3	11.7	13.0
HIP51477	5782	4.03	0.87	0.83	13.7	12.0	15.0
HIP58401	5247	4.67	0.10	0.70	-	-	-
HIP60632	6192	4.31	1.20	0.80	12.1	9.5	14.5
HIP62108	6235	4.18	1.70	0.82	11.8	9.8	12.8
HIP63918	5671	4.17	0.70	0.82	15.8	14.2	17.0
HIP64920	4839	2.53	1.28	1.80	0.8	0.6	1.5
HIP65201	6185	4.39	1.00	0.80	10.5	8.0	13.0
HIP73385	5868	3.90	1.55	0.83	12.3	10.2	14.1
HIP76976	5700	3.20	2.00	1.00	5.0	1.0	15.0
HIP78640	6048	4.22	1.45	0.80	12.8	11.2	14.7
HIP80114	5730	4.24	0.65	0.84	13.4	11.2	15.0
HIP80837	5918	4.16	1.15	0.90	10.5	9.2	11.7
HIP86694	6029	3.83	1.00	0.85	11.1	8.9	13.2
HIP100792	5996	4.31	1.25	0.84	11.6	9.5	14.0

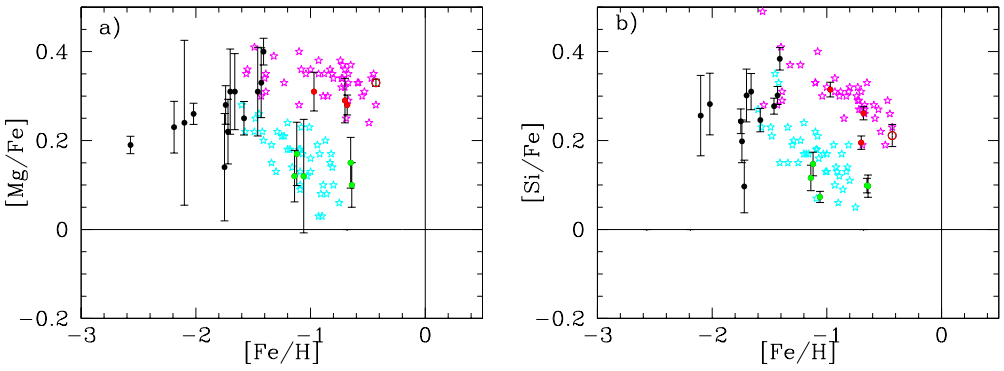

Figure 3.8: Comparison between our sample of halo stars and the halo stars in Nissen and Schuster (2010). The plots show [Mg/Fe] and [Si/Fe] as a function of [Fe/H]. For our sample filled circles are abundances for dwarf stars and the open circle the subgiant HIP64920. The stars that are part of group A are shown in red and the stars in group B in green. The Nissen and Schuster (2010) sample is plotted as open stars, in magenta for the high α stars and cyan for the low α stars.

that the high and low α stars have similar abundances at [Fe/H] $\lesssim -1.5$ and show no separation. This is the same as we can see in our sample for the stars with [Fe/H] $\lesssim -1.5$, where there is no separation into different groups. Our data also extends to lower [Fe/H].

For [Na/Fe] and [Ni/Fe] our sample of halo stars does not show quite the same clear separation between the two groups as in Nissen and Schuster (2010), Figure 3.9. However, the high α-stars have in general high Na and Ni in our sample as well. For [Fe/H] ≥ -1.5 our two trends merge, just as in Nissen and Schuster (2010).

The large spread in [Na/Fe] at $-1.4 \leq$ [Fe/H] ≤ -0.4 for the Nissen and Schuster (2010) sample could indicate that the stars in the three colour coded groups seen in Figure 3.10 have different $T_{\rm eff}$ if Na were sensitive to NLTE (Non-Local Thermodynamic Equilibrium). We conclude that this is not the case since they show similar temperatures in all three groups, Figure 3.10. Thus, to first order, it does not appear likely that different Na abundances are the results of NLTE effects but are real. A comparison between our sample and the Nissen and Schuster (2010) sample shows that our halo stars show a similar separation into two distinct groups as their halo sample. For some of the elements our sample does not show the same clear separation between the stars in the two groups, A and B, as their high and low α stars.

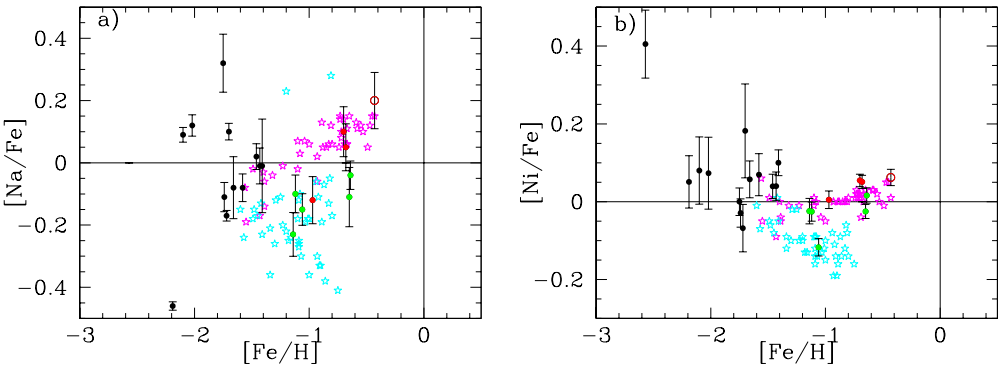

Figure 3.9: Comparison between our sample of halo stars and the halo stars in Nissen and Schuster (2010). The plots show [Na/Fe] and [Ni/Fe] as a function of [Fe/H]. Symbols are as in Figure 3.8.

3.1.8 Comparison with the disk

We now turn to a comparison between our data and a large sample of disk stars. This sample also includes a few halo stars. The data are from Bensby et al. (in prep.). It is important to note that our study uses exactly the same methodology as Bensby et al. (in prep.), hence the comparison is truly differential. We find that the [Mg/Fe] and [Si/Fe] abundances for the stars in group A are similar to the thick disk, Figure 3.11. The two stars with the highest [Fe/He] in group B show similar [Mg/Fe] and [Si/Fe] to the thin disk stars with the lowest [Fe/H]. The halo stars in Bensby et al. (in prep.) show a similar separation for [Fe/H] ≤ -1.5 in [Mg/Fe] and [Si/Fe] as, the groups A and B, in our sample.

Both [Na/Fe] and [Ni/Fe] for the stars in group A are similar to the abundances of the disk, Figure 3.12.

From this we can see that the stars in group A in our sample and the stars with high α-abundances in the Nissen and Schuster (2010) sample have abundances similar those seen in the thick disk of the Milky Way.

3.2 Kinematics

We now turn to look at the kinematics of these two groups of stars, A and B, found in our sample of halo stars. Since our sample is small we will also include the Nissen and Schuster (2010) sample of halo and disk stars, where the halo stars show two distinct populations of stars with high and low α-abundances. Finally we will also include the halo stars, defined as $V_{\rm LSR} < 180 {\rm kms}^{-1}$, from Bensby et al. (in prep.).

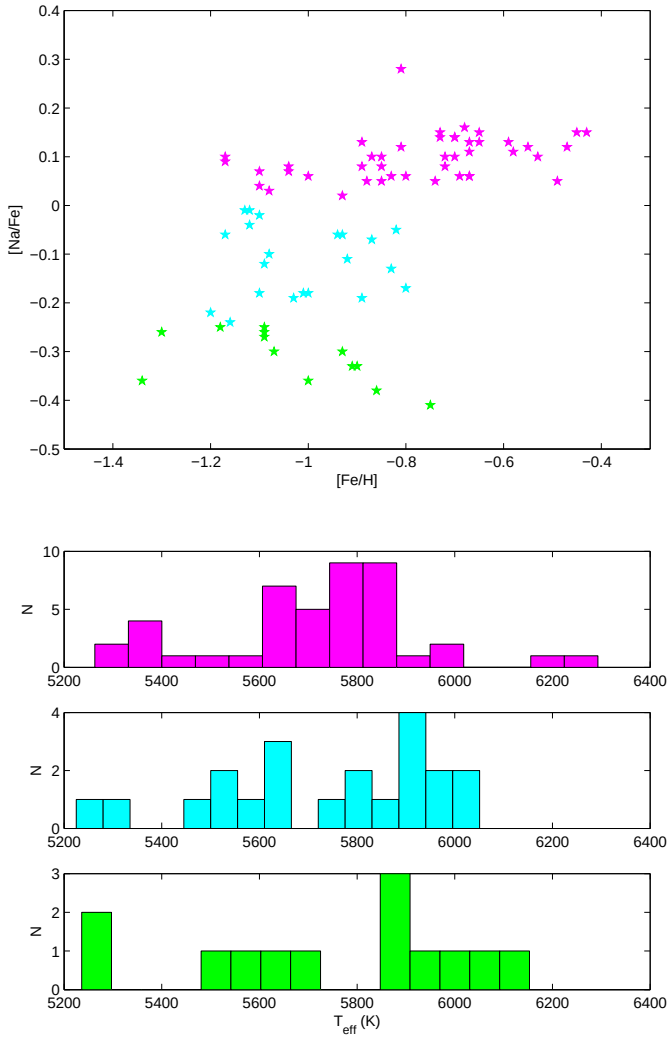

Figure 3.10: Upper: [Na/Fe] as a function of [Fe/H] for a selection of stars in the Nissen and Schuster (2010) sample of halo stars. Filled magenta stars are high α stars, both filled cyan and green stars are low α stars. Lower: Histogram of T_{eff} for the three groups of stars seen to the left. The colours are the same as in the left figure.

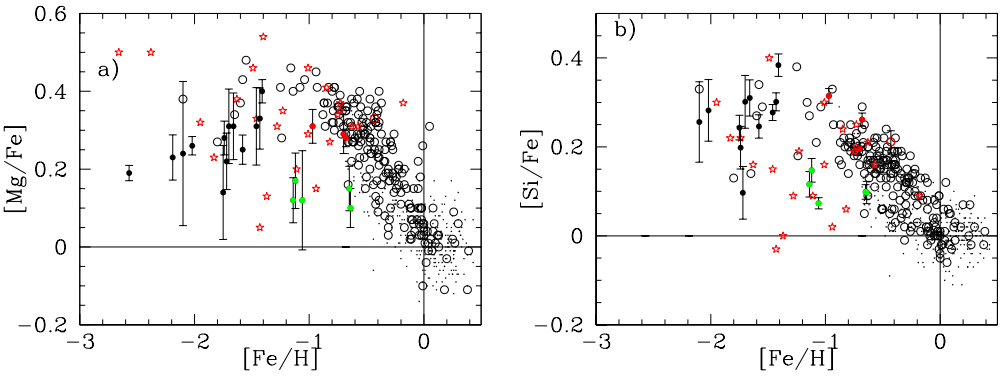

Figure 3.11: Comparison between our sample of halo stars and the halo and disk stars from Bensby et al. (in prep.). The plots show [Mg/Fe] and [Si/Fe] as a function of [Fe/H]. For our sample filled circles are abundances for dwarf stars and the open circle the subgiant HIP64920. The stars that are part of group A are shown in red and the stars in group B in green. For the Bensby et al. (in prep.) sample, small black dots the thin disk, open black circles the thick disk and open red stars the halo.

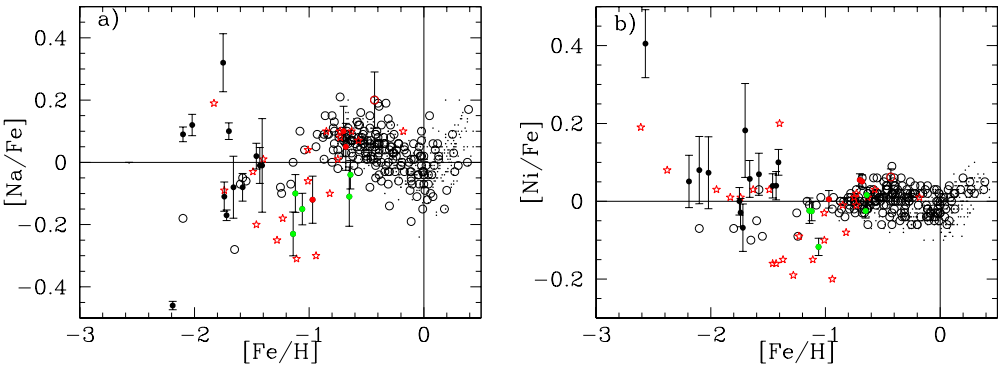

Figure 3.12: Comparison between our sample of halo stars and the halo and disk stars from Bensby et al. (in prep.). The plots show [Na/Fe] and [Ni/Fe] as a function of [Fe/H]. Symbols are the same as in Figure 3.11.

By studying the kinematics of these different populations of stars we can see if there are any significant differences between the two groups of halo stars, which could explain why they show different abundances trends. For example, Nissen and Schuster (1997) proposed that the low α-stars could be the remnants of an accreted smaller galaxy, i.e., part of a stellar stream. Relevant questions to ask are; Have these low α stars kinematics similar to any known streams? The halo stars with high α abundances have abundances similar to the disk stars (Nissen and Schuster, 2010): do they also have kinematics which are similar to the disk stars?

The sample of Nissen and Schuster (2010) is larger than ours and they had another selection criteria giving a larger kinematical spread in their sample.

The best way to study whether the halo stars in our sample and the Nissen and Schuster (2010) sample have kinematics similar to any known stellar stream stars is to look at their angular momenta, $J_{\rm z}$ and $J_{\rm plane}$, since these are intrinsically stable over the whole lifetime of the stars. Additionally, the angular momentum, Figure 3.16 and the Toomre diagram, Figure 3.15, can be used in similar ways to distinguish halo stars from disk stars.

The large separation between the Nissen and Schuster (2010) disk stars and their halo stars seen in the Toomre diagram, Figure 3.15, is not as visible in angular momentum space. This is because the angular momentum in the plane, $J_{\rm plane}$, is most sensitive to velocities perpendicular to the disk, $W_{\rm LSR}$, while the Toomre diagram depends on both $U_{\rm LSR}$ and $W_{\rm LSR}$. $W_{\rm LSR}$ is not as high as $U_{\rm LSR}$ for stars with $V_{\rm LSR}$ velocities similar to the disk stars, which means that they would not be as prominent in angular momentum space as in the Toomre diagram.

In angular momentum space, 70% of the stars from Nissen and Schuster (2010) with high α abundances (filled magenta stars) show a prograde rotation. Out of these 70% around 50% show kinematic features in angular momentum space which are similar to those of the disk. Meanwhile the stars with low α abundances (filled cyan stars) are more kinematically similar to the halo.

The stars which Nissen and Schuster (2010) showed to have high α abundances are generally close to the disk according to their kinematics, especially their $V_{\rm LSR}$. The stars that have low α abundances have, in general, lower $V_{\rm LSR}$, i.e. they are lagging behind the disk. These low α stars also have a large scatter in their $U_{\rm LSR}$.

We begin by studying if there are any significant differences between the velocities, $U_{\rm LSR}$, $V_{\rm LSR}$ and $W_{\rm LSR}$, for the different samples of stars, Figure 3.13 and 3.14.

All stars in our sample have $V_{\rm LSR} \leq -150{\rm kms}^{-1}$, they show a larger spread in $U_{\rm LSR}$ than in $W_{\rm LSR}$. The star which stands out from the rest is

HIP16404. It has a low $V_{\rm LSR}$ which gives rise to a very low $J_{\rm z}$ value, for further discussion see Section 3.3.1.

The Nissen and Schuster (2010) sample shows a larger spread in $V_{\rm LSR}$ than our sample. This is mainly due to differences in the selection criteria. A large portion of their halo stars with high α-abundances have $V_{\rm LSR}$ similar to the $V_{\rm LSR}$ of their disk stars, Figure 3.13 and 3.14. The $U_{\rm LSR}$ and $W_{\rm LSR}$ velocities are similar to our sample, with the exceptions of a few outliers. Six of the low α stars in the Nissen and Schuster (2010) sample have very low $U_{\rm LSR}$, Figure 3.13. However, these six stars do not show extreme kinematics in angular momentum space similar to any known streams. This is the case for the two binary stars, HIP37670 and HIP37671, with low $W_{\rm LSR}$ velocities, Figure 3.14, which have $J_{\rm plane}$ similar to the Helmi et al. (1999) stream, for further discussion see Section 3.3.2.

One thing to point out is that, for both our sample and the Nissen and Schuster (2010) sample of halo stars, a large fraction of the stars have positive $U_{\rm LSR}$ velocities. This is not seen for the stars in the Schuster catalouge (Schuster et al., 2006), shown as small black dots in Figure 3.13 to 3.16. The Schuster et al. (2006) catalogue contains uvby-photometry for 442 high-velocity and metal-poor stars, and based on Hipparcos parallaxes the absolute magnitude have been calculated. This will later be used for colour-magnitude diagrams of possible stream stars, Section 3.3.

With regards to the kinematics there are, in general, no large differences between the stars in group A and B, either according to their velocities, in the Toomre diagram, Figure 3.15, or in angular momentum space, Figure 3.16.

3.2.1 HIP22060

When categorizing stars, e.g. if they are members of the halo or the disk, the categorization may differ depending on the method used. One example is HIP22060. Nissen and Schuster (2010) have categorized it as a halo star according to the criteria that a halo star would have $V_{\rm tot} \geq 180$kms^1. However, a categorization based on $J_{\rm z}$ and $J_{\rm plane}$ would have categorized it as a disk star, Figure 3.16. Indeed, twelve out of the sixteen disk stars in the Nissen and Schuster (2010) sample have kinematics more similar to the halo, in $J_{\rm z}$ and $J_{\rm plane}$, than HIP22060. Hence, this star would more probably be a member of the disk than the halo.

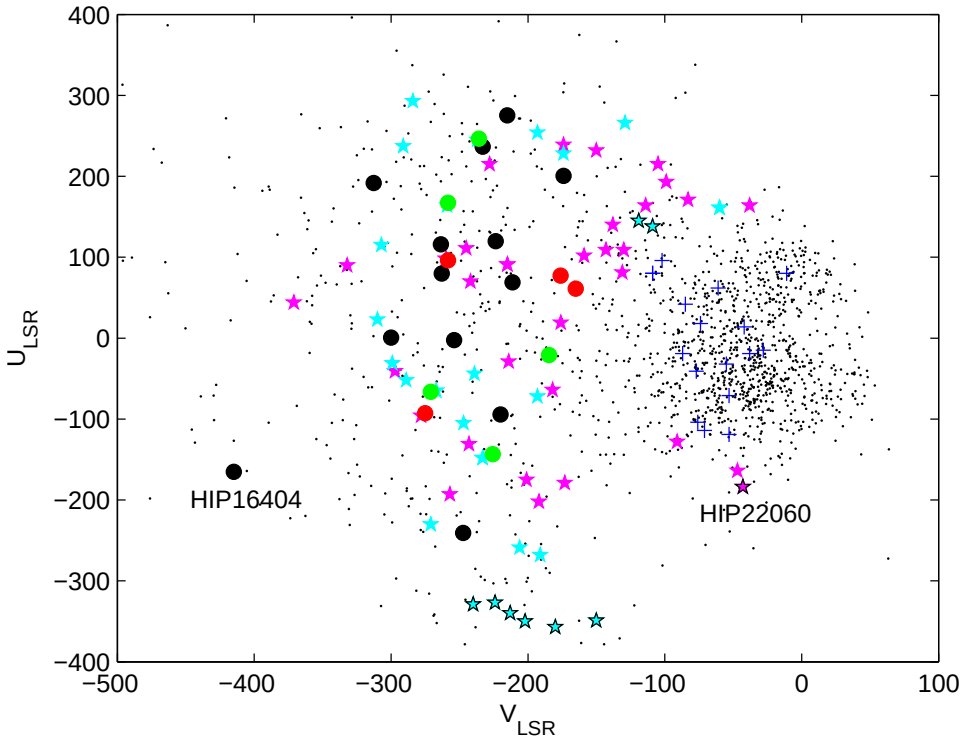

Figure 3.13: $U_{\rm LSR}$ against $V_{\rm LSR}$. The small black dots are the stars in the Schuster et al. (2006) catalogue . The filled red and green circles are the stars in groups A and B, the black filled circles are the rest of the stars in our sample of halo stars. The blue crosses are the disk stars in the Nissen and Schuster (2010) sample and the filled stars are the halo stars, cyan and magenta are the low and high α stars. The stars with low $U_{\rm LSR}$ or $W_{\rm LSR}$ are marked with a black border.

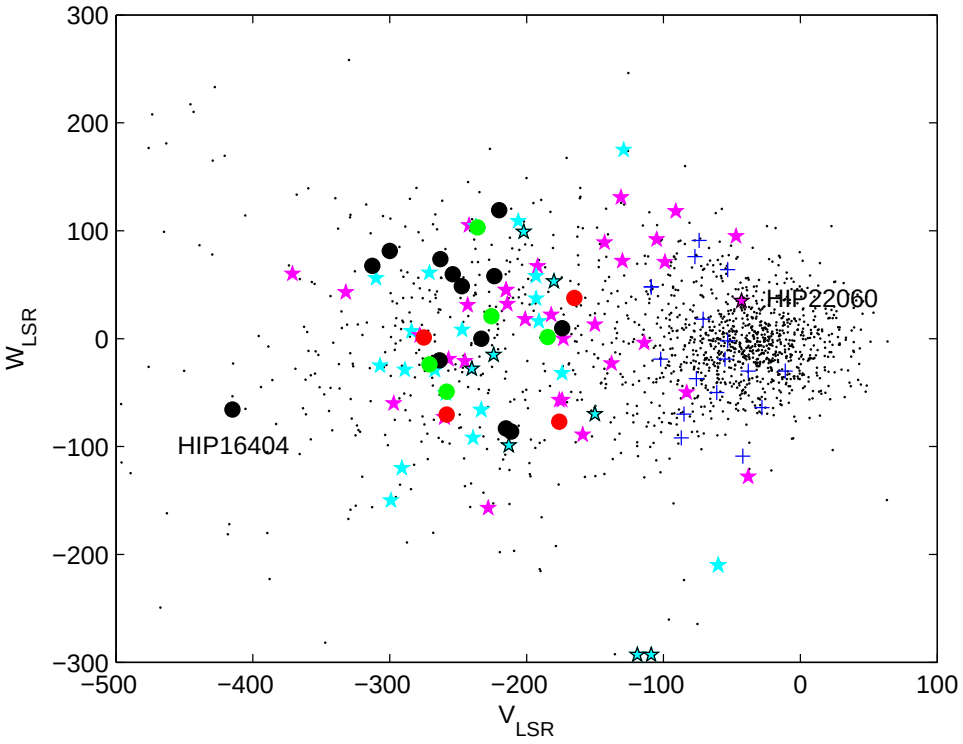

Figure 3.14: U_{LSR} against V_{LSR}. Symbols are the same as in Figure 3.13.

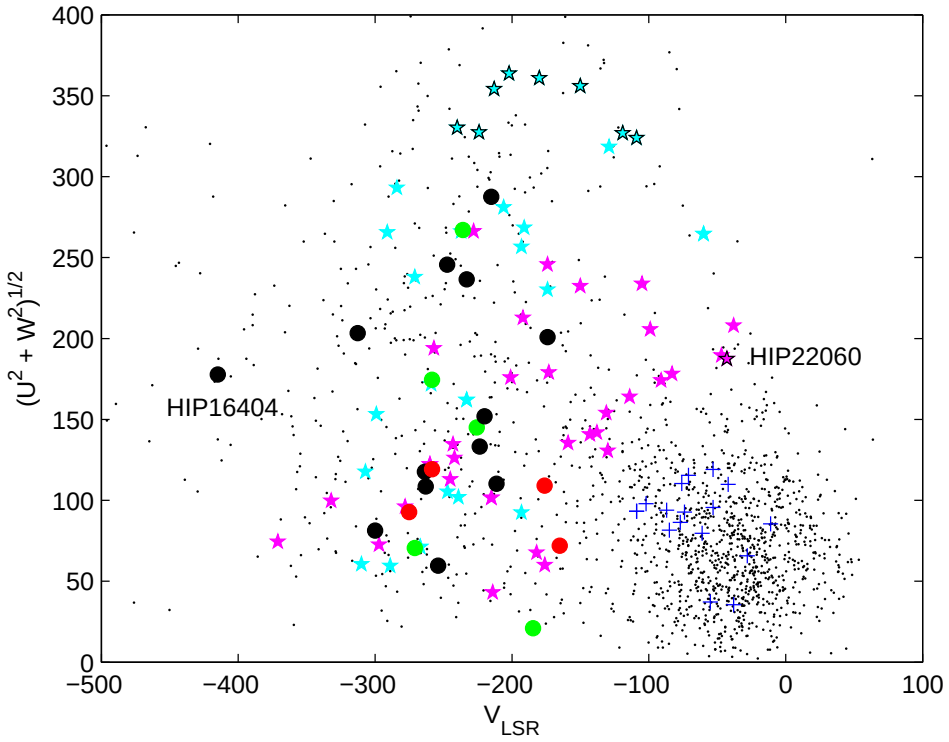

Figure 3.15: The Toomre diagram for the stars in our sample and the Nissen and Schuster (2010) sample. Symbols are the same as in Figure 3.13.

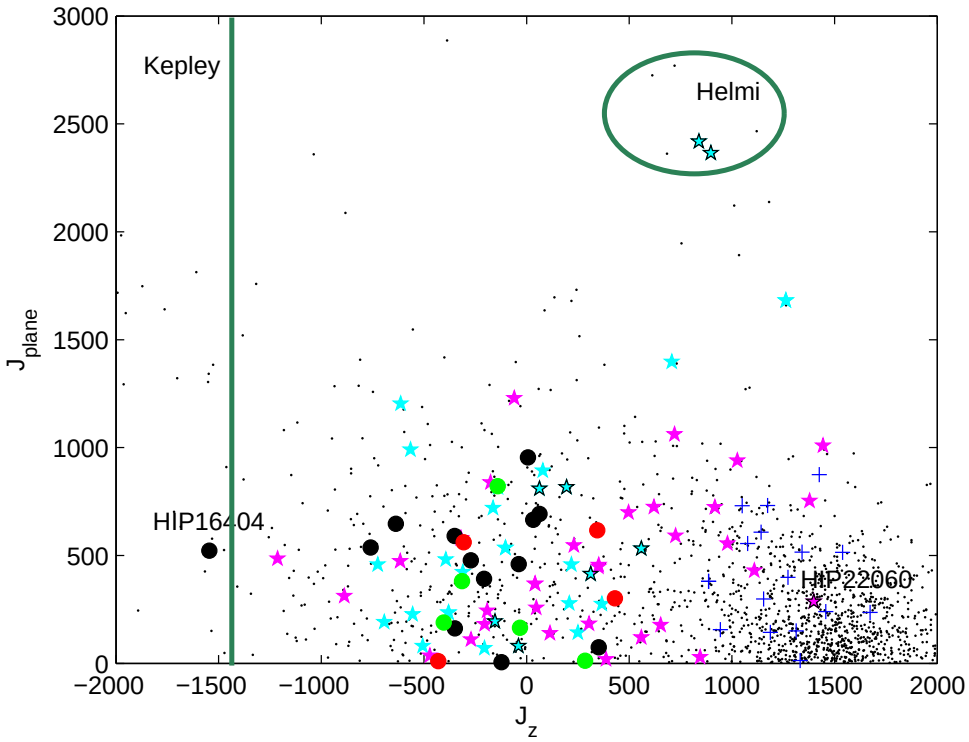

Figure 3.16: The angular momenta for the stars in our sample and the Nissen and Schuster (2010) sample. Symbols are the same as in Figure 3.13. The stars to the left of the green line have J_z similar to the stream in Kepley et al. (2007). The green ellipse indicate where the stars in the Helmi et al. (1999) stream are found.

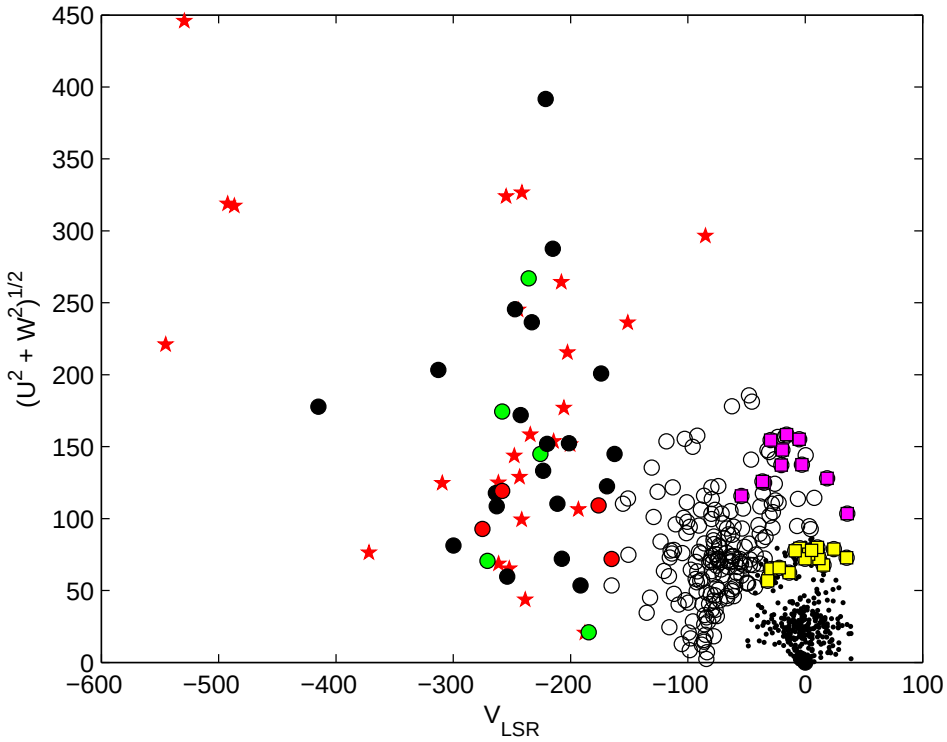

Figure 3.17: Toomre diagram for the halo stars in our sample and the dwarf stars (halo and disk) in Bensby et al. (in prep.). Filled red and green circles are the stars in groups A and B, the filled black circles are the rest of the our halo sample. Small black dots are the thin disk stars, open black circles are the thick disk stars and red filled stars are halo stars from Bensby et al. (in prep.). Yellow filled squares are the thick disk stars which overlap the thin disk stars in the Toomre diagram. The filled magenta squares are the thick disk stars which overlap the thin disk in angular momentum space.

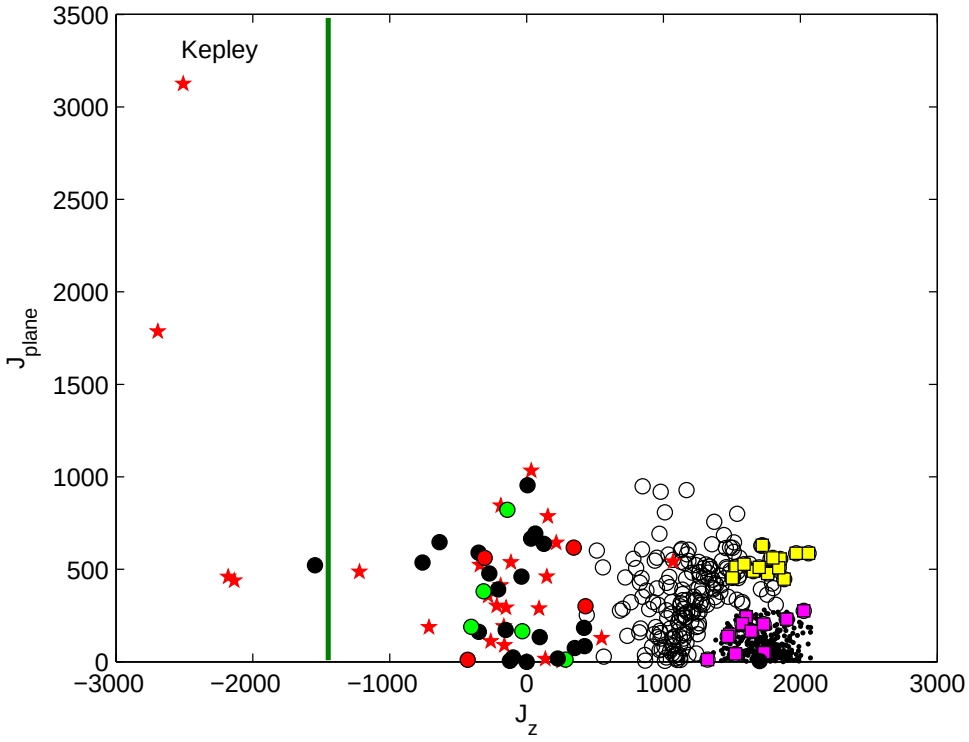

Figure 3.18: Angular momentum space for halo stars in our sample and the dwarf stars (halo and disk) in Bensby et al. (in prep.). Symbols are the same as in Figure 3.17.

3.2.2 The transition between the two disks

In a comparison with the dwarf stars from Bensby et al. (in prep), which consist mainly of disk stars, we see that our halo stars have very different kinematics compared to the stars belonging to the disk, Figure 3.17 and 3.18.

The halo stars in Bensby et al. (in prep), show similar kinematics to our sample of halo stars, Figures 3.17 and 3.18. They also show similar elemental abundances to our sample of halo stars, Figure 3.19. The Bensby et al. (in prep) halo stars show the same type of separation into two groups for the α-elements, as group A and B. Four of the halo stars in Bensby et al. (in prep.), HIP58962, HIP74235, HIP74235 and HIP90261, have very low J_z, ≤ -2000, which puts them in the same J_z, $J_{\rm plane}$ region as the retrograde stream found by Kepley et al. (2007), Figure 3.18. Three of these stars have low [Si/Fe] abundances and one has high [Si/Fe] similar to our halo stars in group A, Figure 3.19.

One other feature seen in Figure 3.17 and 3.18, are those thick disk stars (open circles) which are located in the same region as the thin disk stars (black dots) both in angular momentum space and in the Toomre diagram. These thick disk stars are marked as filled yellow squares if they have kinematics similar to the thin disk in the Toomre diagram and as filled magenta squares if they have similar kinematics to the thin disk in angular momentum space. It is clear, in Figure 3.17 and 3.18, that these stars are not the same in the two cases. This can be explained by different velocities in $U_{\rm LSR}$ and $W_{\rm LSR}$ for the two cases, since $J_{\rm plane}$ is most sensitive to $W_{\rm LSR}$ while in the Toomre diagram the position of the y-axis depends both on $U_{\rm LSR}$ and $W_{\rm LSR}$, since $(U^2_{\rm LSR} + W^2_{\rm LSR})^{1/2}$. From this we see that the thick disk stars overlapping the thin disk in angular momentum space (magenta squares) have smaller $W_{\rm LSR}$ velocities than the ones overlapping in the Toomre diagram (yellow squares), since they have a much lower $J_{\rm plane}$ value. But we can also see that these stars (magenta squares) have larger $U_{\rm LSR}$ since they show higher $(U^2_{\rm LSR} + W^2_{\rm LSR})^{1/2}$ than the other overlapping group of stars in the Toomre diagram.

We conclude that it is not sufficient to only use one selection method to categorize stars as members of the thick or the thin disk. This is similar to the discussion in the previous section, Section 3.2.1, regarding the star HIP22060 which can be categorized to be a halo or a disk star depending on method used.

The [Si/Fe] abundances for these two types of overlapping stars, Figure 3.19 are similar to both the thick and the thin disk abundances. The stars overlapping the thin disk in the Toomre diagram (yellow squares) generally show abundances similar to the thin disk and the overlapping stars in angular momentum space (magenta squares) have abundances similar to the thick

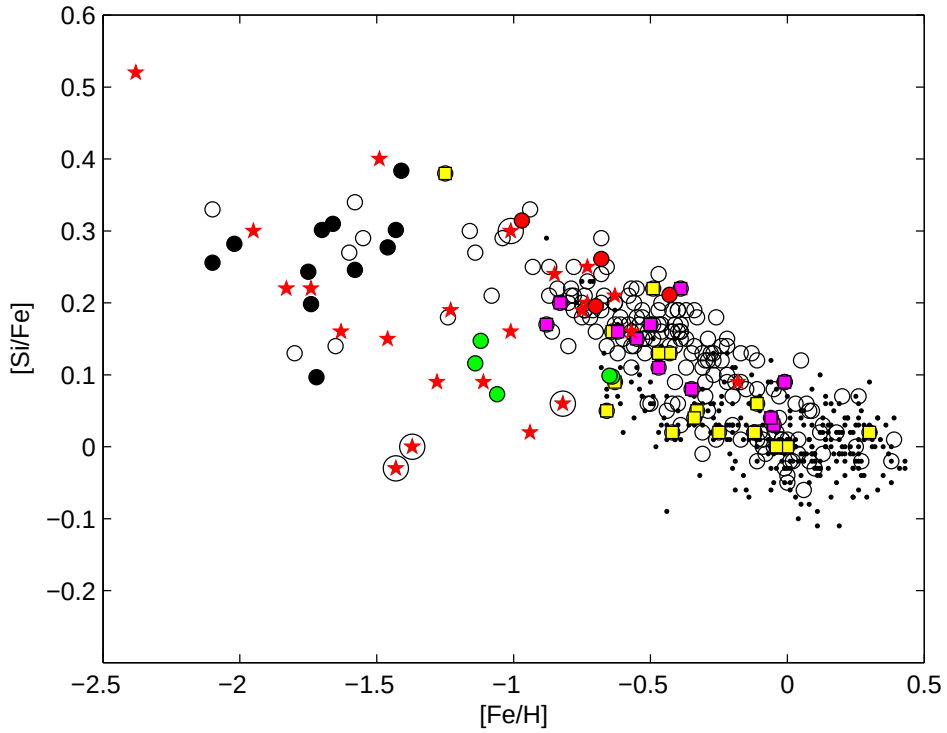

Figure 3.19: [Si/Fe] as a function of [Fe/H] halo stars in our sample and the dwarf stars (halo and disk) in Bensby et al. (in prep.). Symbols are the same as in Figure 3.17. The four halo stars in Bensby et al. (in prep.) which are potential stream stars are marked with a large open black circle.

disk, i.e. higher [Si/Fe] ratios for a given Fe, but there is still an overlap between these two groups of overlapping stars.

From both the velocity differences and the differences between the [Si/Fe] abundances for these two groups of overlapping stars, we conclude that the stars which have abundances similar to the thin disk (yellow squares) have larger $W_{\rm LSR}$, velocities perpendicular to the disk, and smaller $U_{\rm LSR}$ than the stars with abundances similar to the thick disk. This means that these stars, yellow squares, have over the whole group a more puffed up path around the Milky Way than normal thin disk stars, i.e they follow more the path of the thick disk.

3.3 Potential stream members

3.3.1 New potential members of the Kepley stream

The stellar stream found by Kepley et al. (2007) consists of stars with retrograde rotation, i.e., very low J_z and V_{LSR}, Figure 3.16. In our sample of halo stars, the star HIP16404 has a low J_z similar to the retrograde stellar stream (Kepley et al., 2007). HIP16404 is one of the most metal-poor stars in our sample with [Fe/H]$= -2.19$.

As seen in Figure 3.16 four halo stars from Bensby et al. (in prep.) have J_z similar to the Kepley et al. (2007) stream. These four stars are listed in Table 3.2. We find that a few stars from Schuster et al. (2006) catalogue also show low J_z values, Figure 3.16. Table 3.2 lists these stars which are all new potential members of the Kepley et al. (2007) stream. All of these stars have [Fe/H]< -1 (photometric) and some have [Fe/H] similar to HIP16404.

From the histogram , Figure 3.20, of the metallicities of the new potential stream stars from the Schuster et al. (2006) catalogue it is clear that it consists of two different populations of stars. One of the populations has a metallicity of [M/H] ≥ -2 and the other has [M/H] < -2. These two populations are shown in the colour-magnitude diagram, Figure 3.21, and in the Strömgren c_1 versus colour plots, Figure 3.22 and 3.23. From these figures we conclude that with the help of the Dartmouth [1] isochrones[2] we estimate a minimum age of ~ 11 Gyr for both the metal-rich and metal-poor populations of new possible stream stars.

3.3.2 New potential members of the Helmi Stream

The two binary stars, HIP37670 and HIP37671, in Nissen and Schuster (2010) have low W_{LSR} velocities and J_{plane} similar to the Helmi et al. (1999) stream. These two stars have [Fe/H] $= -1.29$ and [Fe/H] $= -1.25$ respectively. Both stars have low α-abundances and low Na and Ni abundances.

In Morrison et al. (2009) the stars which have similar angular momentum as the Helmi et al. (1999) stream have $-2.5 \leq$[Fe/H] ≤ -1, Figure 1.3. The twelve stars in Roederer et al. (2010) have metallicities between $-3.35 \leq$[M/H] ≤ -1.45. However, it seems that these twelve stars fall into three different populations of stars according to their metallicities, [M/H] ~ -1.5, $-2.5 \leq$[M/H] ≤ -2.1, and [M/H]≤ -3.2.

In the Schuster et al. (2006) catalogue there are four more possible stream stars, Figure 3.16. These four stars have [M/H]≥ -1.72 and are clearly part

[1] stellar.dartmouth.edu/∼models

[2] Evolutionary tracks of a stellar population at a specific age and metallicity

Table 3.2: New potential members of the Kepley et al. (2007) stream. Columns two, three, and six are taken from SIMBAD. Column four lists the photometric metallicity from the Schuster et al. (2006) catalouge. Column five lists [Fe/H] (Bensby et al. (in prep.)).

Name	RA	Dec	[M/H]	[Fe/H]	Sp. type
HIP5445	01 09 43.0639	+61 32 50.201	-1.58	-	F8V
HIP15396	03 18 28.9152	-07 08 25.638	-2.05	-	A6
G196-047	10 50 29.11	+56 26 30.9	-1.53	-	G8
HIP106468	21 33 49.7529	-35 26 14.235	-2.67	-	B8
G016-035	16 12 50.64	+06 43 55.8	-1.32	-	K
LP714-049	04 18 34.514	-13 12 27.18	-1.12	-	-
LP739-005	13 59 18.617	-13 42 42.41	-1.88	-	-
G020-019	17 53 58.63	+03 03 16.3	-1.83	-	-
HIP46516	09 29 15.5626	+08 38 00.476	-2.16	-	A0
HIP68592	14 02 30.0902	-05 39 05.213	-2.27	-	A2s
G075-056	03 00 23.028	-05 57 49.48	-1.99	-	G
HIP27111	05 44 56.7890	+09 14 31.490	-1.64	-	F8
G117-064	10 01 22.79	+28 46 02.5	-1.82	-	-
G137-086	16 10 15.24	+09 08 22.0	-1.13	-	-
HIP83320	17 01 43.9816	+16 09 03.352	-2.46	-	sd:F
G140-039	18 06 47.74	+10 52 33.6	-	-	G
G167-050	15 35 31.55	+27 51 02.2	-1.98	-	-
HIP85855	17 32 41.6250	+23 44 11.631	-2.18	-	G0
G199-066	13 20 31.28	+56 34 48.3	-1.49	-	-
HIP116782	23 40 03.0164	-19 27 27.829	-1.64	-	F2
HIP58962	12 05 24.8515	-26 35 43.772	-	-0.82	sdF8
HIP74234	15 10 12.9679	-16 27 46.517	-	-1.37	K0V
HIP74235	15 10 13.0872	-16 22 45.854	-	-1.43	K0/K1V
HIP90261	18 25 01.8475	-45 28 47.388	-	-1.01	F8

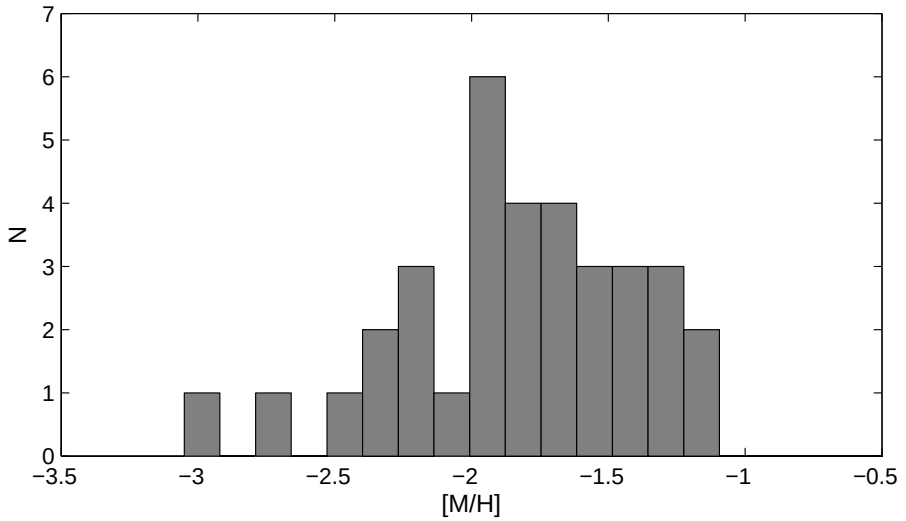

Figure 3.20: Histogram of the metallicities of the new potential stream stars in the Kepley et al. (2007) stream.

of the metal-rich population of stars in the Helmi et al. (1999) stream. The two stars from Nissen and Schuster (2010) and the four stars from the Schuster et al. (2006) catalogue are shown in the colour-magnitude diagram and in the c_1 plot, and compared with isochrones from Dartmouth. We estimated an age of between 11-13 Gyr for four of the stars. HIP43099 is younger at $\sim$ 5 Gyr, Figure 3.24 and 3.25. Compared to the new potential stream stars for the Kepley et al. (2007) stream, the stars in the Helmi et al. (1999) stream are younger according to the evolutionary tracks. This is expected from the metallicities since the new potential stream stars in the Helmi et al. (1999) stream are more metal-rich than the new potential stream stars in the Kepley et al. (2007) stream.

3.4 The Ni and Na relation

Nissen and Schuster (2010) point out a relation between Na and Ni. Here we combine their data with ours and the stars from Bensby et al. (in prep.). Figure 3.26 clearly shows that there is a correlation between Ni and Na. The two stars in the Nissen and Schuster (2010) sample that do not follow the correlation with much higher [Na/Fe] abundances than the other low α stars are G150-40 and G53-41, Figure 3.26.

This correlation can not be explained from enrichment by Supernovae type Ia, because type Ia supernovae hardly produce any Na. In Nissen &

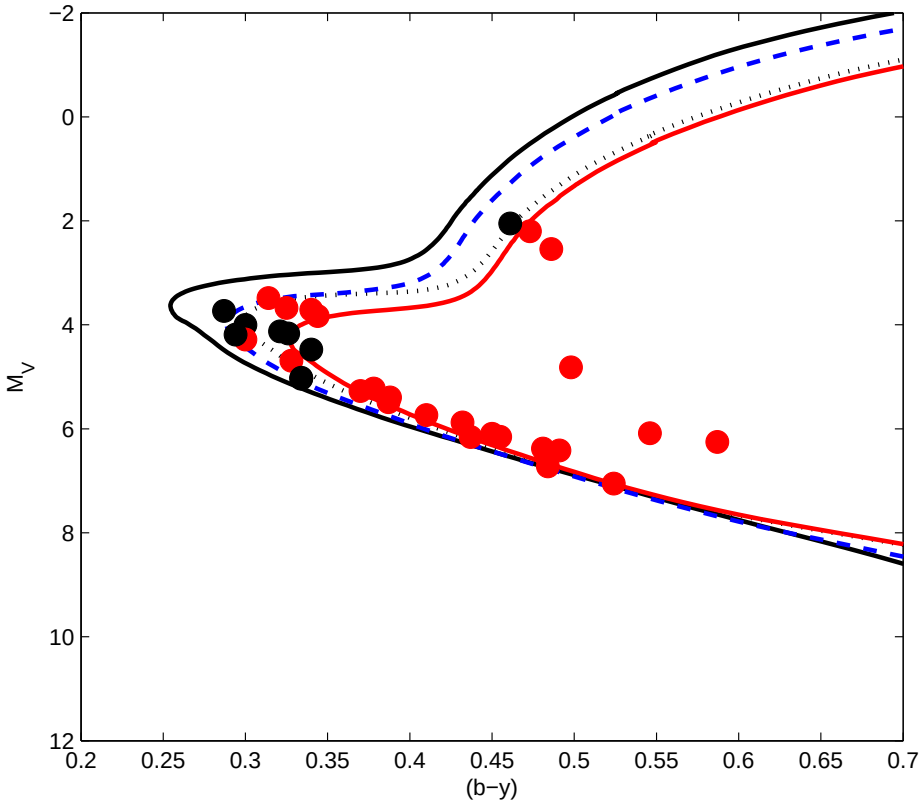

Figure 3.21: Colour-Magnitude diagram for the new potential Kepley et al. (2007) stream stars. Red filled circles show the metal-rich population, and the black filled circles the metal-poor population. Isochrones for different ages and metallicities: black solid line 11 Gyr and [Fe/H] = -2.0, blue dashed line 13 Gyr and [Fe/H] = -1.5, black dotted line 11 Gyr and [Fe/H] = -1.0, and red solid line 15 Gyr and [Fe/H] = -1.0.

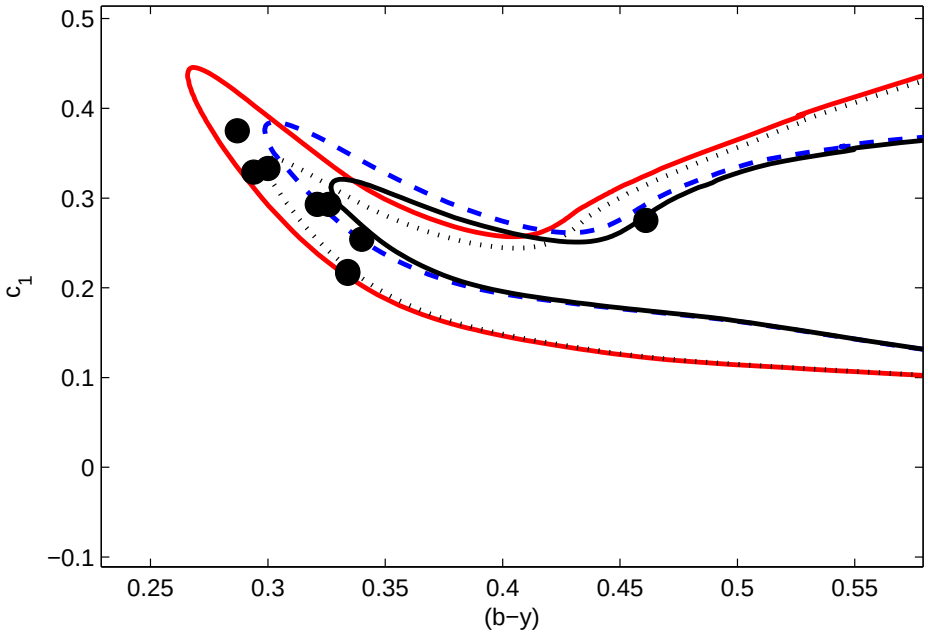

Figure 3.22: The Strömgren c_1 index as a function of colour. The black filled circles show the metal-poor population. Isochrones for different ages and metallicities: black solid line 15 Gyr and [Fe/H] = -1.0, blue dashed line 11 Gyr and [Fe/H] = -1.0, black dotted line 15 Gyr and [Fe/H] = -2.0, and red solid line 11 Gyr and [Fe/H] = -2.0.

Table 3.3: New potential members of the Helmi et al. (1999) stream. Columns two, three, and six are taken from SIMBAD. Column four lists the photometric metallicity from the Schuster et al. (2006) catalogue. Column five lists [Fe/H] (Nissen and Schuster, 2010).

Name	RA	Dec	[M/H]	[Fe/H]	Sp. type
HIP46120	09 24 20.9738	-80 31 21.294	-1.72	-	sdG
G025-024	21 16 42	-01 18.2	-1.67	-	G
HIP43099	08 46 39.5764	-13 21 25.389	-1.48	-	A5
G166-037	14 34 51.11	+25 10 03.6	-1.55	-	-
HIP37670	07 43 44.0828	-00 03 49.201	-1.23	-1.29	sdF
HIP37671	07 43 43.9593	-00 04 00.948	-1.49	-1.25	sdF

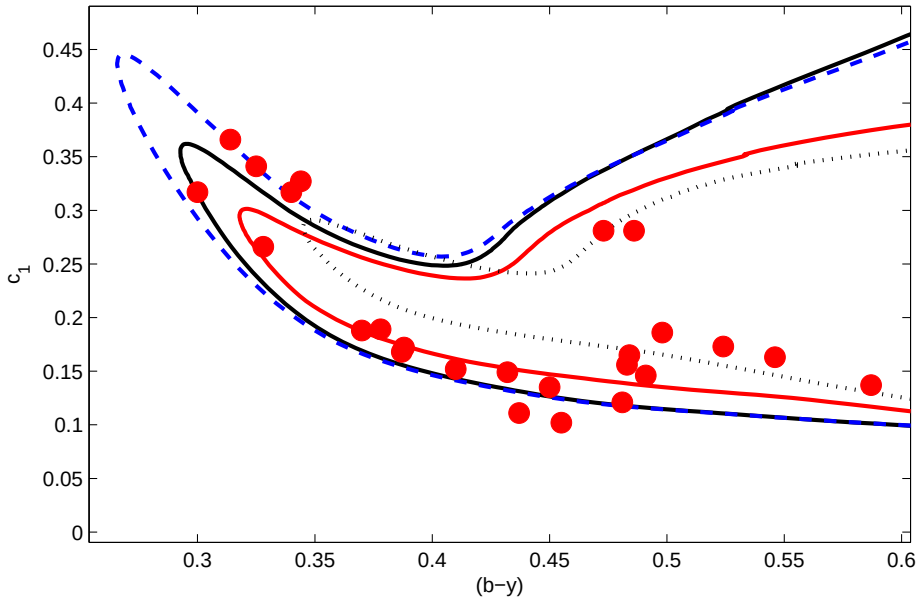

Figure 3.23: The Strömgren c_1 index as a function of colour. The red filled circles show the metal-rich population. Isochrones for different ages and metallicities. Black solid line 15 Gyr and [Fe/H] = -2.0, blue dashed line 11 Gyr and [Fe/H] = -2.0, black dotted line 15 Gyr and [Fe/H] = -1.0, and red solid line 15 Gyr and [Fe/H] = -1.5.

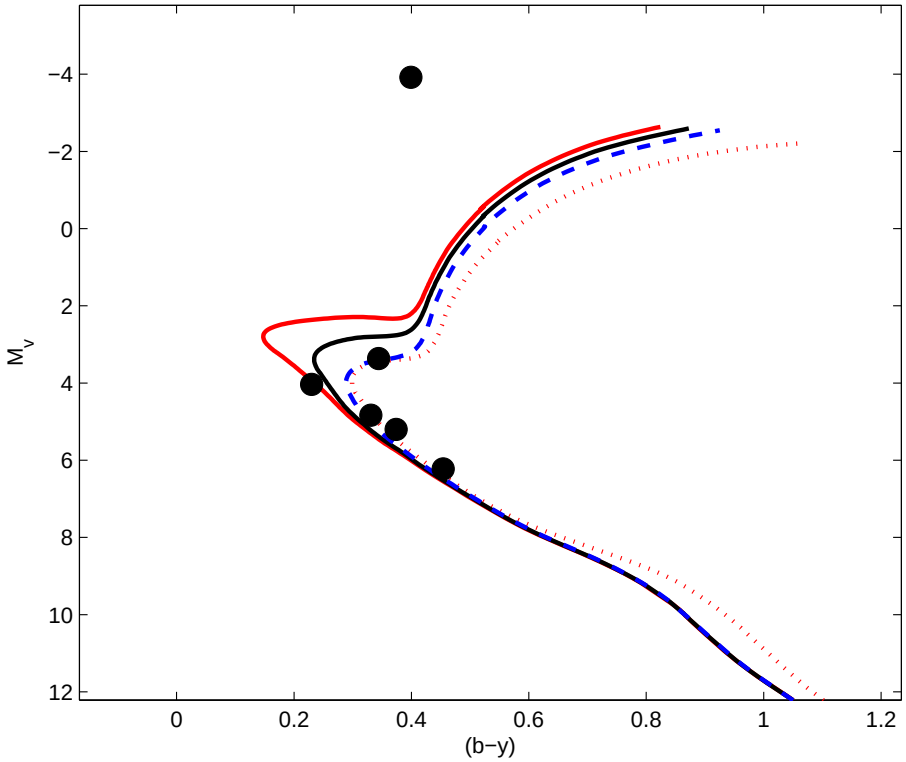

Figure 3.24: Colour-Magnitude diagram for the new potential Helmi et al. (1999) stream stars, filled black circles. Isochrones for different ages and metallicities. Red solid line 5Gyr and [Fe/H] = -1.0, black solid line 8Gyr and [Fe/H] = -1.5, red dotted line 11Gyr and [Fe/H] = -1.0, and blue dashed line 13Gyr and [Fe/H] = -1.5.

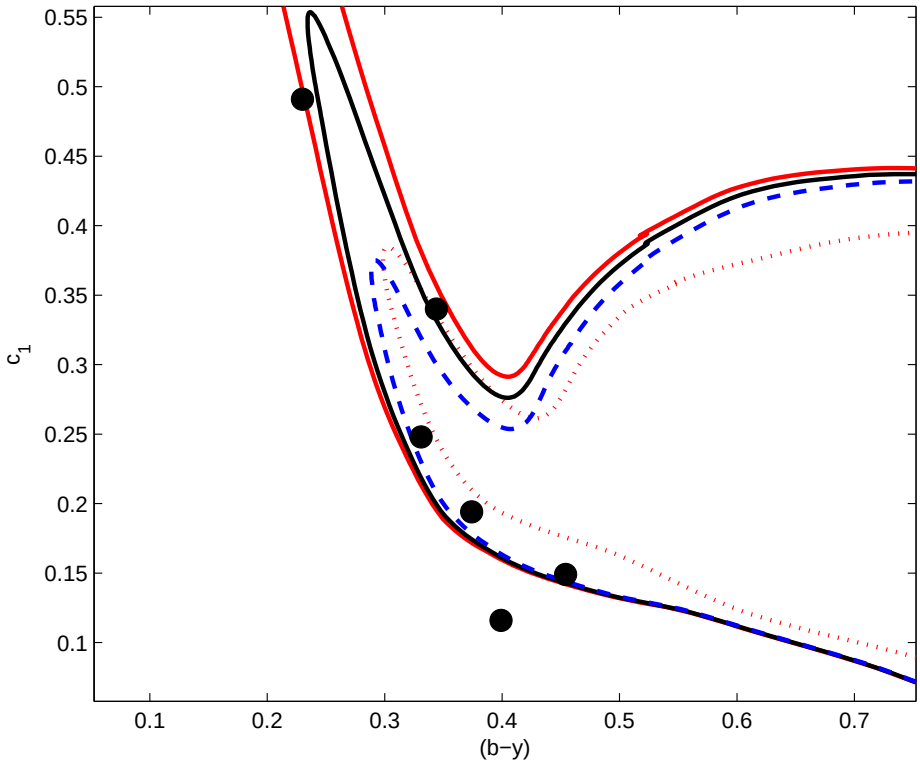

Figure 3.25: The Strömgren c_1 index as a function of colour, filled black circles. Isochrones for different ages and metallicities. Red solid line 5Gyr and [Fe/H] = -1.0, black solid line 8Gyr and [Fe/H] = -1.5, red dotted line 11Gyr and [Fe/H] = -1.0, and blue dashed line 13Gyr and [Fe/H] = -1.5.

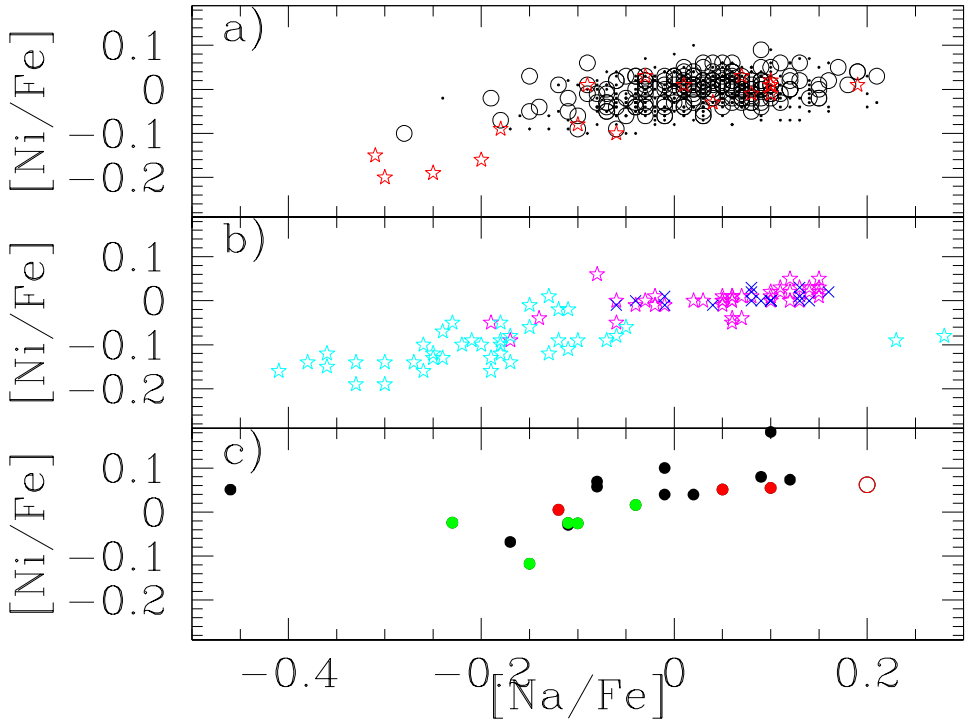

Figure 3.26: The [Ni/Fe] as a function of [Na/Fe]. a) The disk stars from Bensby et al. (in prep.). b) The sample of stars from Nissen and Schuster (2010), where the crosses are the disk stars and the stars the halo stars, cyan open stars are the low α stars and magenta the high α stars. c) Our sample of halo stars. The filled red and green circles are the the stars in groups A and B. The black filled circles are the rest of the sample.

Schuster (1997) they argued that this correlation between Ni and Na could be due to the fact that ^{56}Ni and Na both depend on the neutron excess within the stellar interior. The neutron excess is thought to depend on the heavy element abundances, including the α-elements. The idea is that type II supernovae control the correlation between Ni and Na after the first type Ia supernovae have started to modify the [α/Fe] ratio. This might also explain why Ni and Na correlate more closely with the α-elements than with iron.

Nissen and Schuster (2010) found that the stars with lower [Na/Fe] have a large scatter in their U_{LSR} velocities, shown in Figure 3.27. This seems also to be the case for the disk stars in Bensby et al. (in prep.), where the few stars with low [Na/Fe] ratios have the most extreme U_{LSR}. For our sample of 23 halo stars it is not possible to draw any such conclusions. However, our sample is compatible with the Nissen and Schuster (2010) sample and does

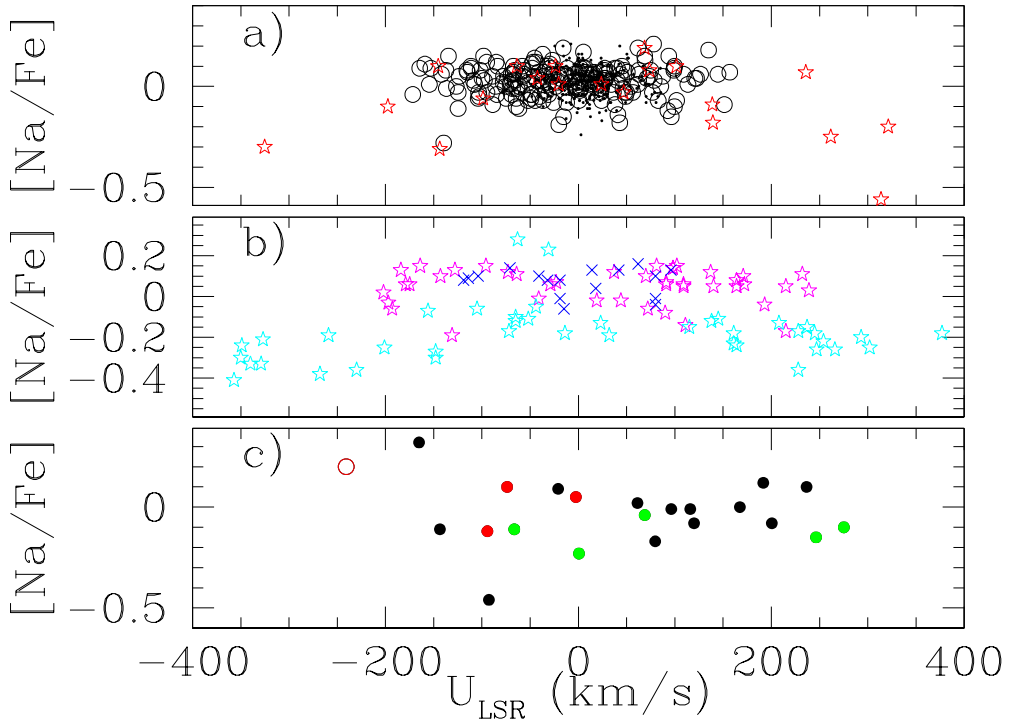

Figure 3.27: [Na/Fe] as a function of U_{LSR}. The symbols are the same as in Figure 3.26.

not show any stars which deviate from their results.

For [Mg/Fe] the Nissen and Schuster (2010) sample also shows evidence that the stars with lower [Mg/Fe] abundances (α - abundances) are more likely to have more extreme U_{LSR} velocities. For our sample of halo stars we can conclude that they follow the general trend seen in the Nissen and Schuster (2010) sample. The disk stars do instead show something different, seen in Figure 3.28. Here it is the stars with enhanced [Mg/Fe] abundances that have a larger scatter of the U_{LSR} velocities..

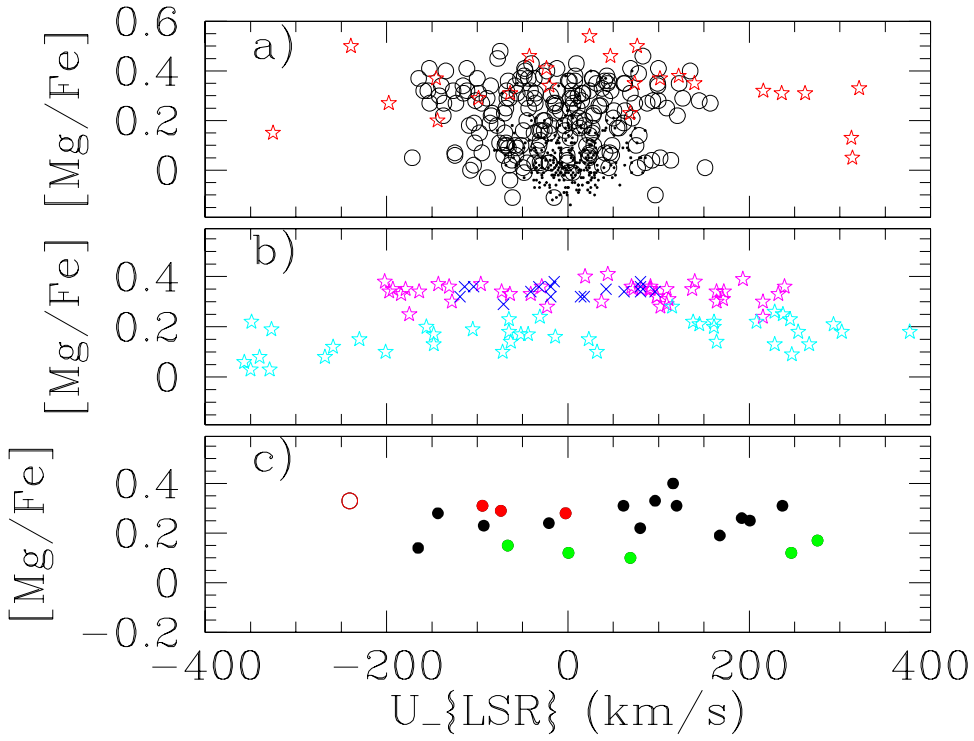

Figure 3.28: [Mg/Fe] as a function of U_{LSR}. The symbols are the same as in Figure 3.26.

Chapter 4

Summary and Discussion

We have shown that the separation in abundances, especially the α -elements, seen in halo stars with $-1.5 \leq$ [Fe/H] ≤ -0.5 by Nissen and Schuster (1997) is also present in our sample of halo stars. For [Mg/Fe] and [Si/Fe] this separation is obvious, for [Ca/Fe] and [Ti/Fe] it is not as prominent in our sample as in the Nissen and Schuster (2010) sample. However, we still see that the stars which have higher abundances of [Mg/Fe] and [Si/Fe], group A, have higher [Ca/Fe] and most of the stars have higher [Ti/Fe] abundances than the stars in group B at similar [Fe/H].

Nissen and Schuster (1997, 2010) showed that these stars with high abundances of α-elements also have higher abundances of [Na/Fe] and [Ni/Fe] than the stars with low α-abundances. Our sample of halo stars shows similar separation in [Na/Fe] and [Ni/Fe] abundances for most of the stars in group A and B, Figure 3.9. However, one star in group A has [Na/Fe] similar to the stars in group B and two stars in group B have [Ni/Fe] abundances similar to both the stars in group A and the high α-abundance stars in Nissen and Schuster (2010). What is more interesting is that we also see a separation between the stars in group A and B in the [Zn/Fe] abundances, Figure 3.7. This has not been seen in any previous studies. For our sample of halo stars the separation in the [Zn/Fe] abundances is more clear than the separation in [Na/Fe] and [Ni/Fe]. It would therefore be interesting to know if this separation is also present in the Nissen and Schuster (2010) sample. One explanation of why Zn would separate in the same way as Mg and Si could be its formation process. Zn is produced by explosive Si burning and slow neutron capture (Cayrel et al., 2004). The production of Zn will therefore depend on the amount of Si and metallicity of the star, which could explain the similar seperation in [Zn/Fe] and [Si/Fe].

The stars in group A and the high α-abundance stars in the Nissen and Schuster (2010) sample have abundances similar to the thick disk of the Milky

Way (Nissen and Schuster, 2010; Bensby et al., in prep.). As can be seen in Figure 3.13 to 3.16, these stars, especially the high α stars, show kinematics similar to the disk. The main difference is the V_{LSR} velocity which is smaller for the high α stars than for the disk stars in the Nissen and Schuster (2010) sample. One explanation could be that these halo stars have formed in similar ways to the disk and due to radial migration have gained velocities associated with the halo. This process follows the formation of the thick disk from the thin disk in the theoretical model of Schönrich and Binney (2009a, 2009b). If the velocity distribution of the thick disk is non-Gaussian with an extended tail towards high velocities as in the model of Schönrich and Binney (2009b), then the high α stars with $180 < V_{tot} < 210$ km s^{-1}, corresponding to half of the high α stars, could belong to the same population of stars as the thick disk (Nissen and Schuster, 2010). However, the stars in group A in our sample and half of the high α stars in Nissen and Schuster (2010) have $V_{tot} > 210$ km s^{-1}, and they show a well-defined trend which is separated from the low α stars.

The two groups of stars separated in abundances do not have large differences in their kinematics. The stars with low α abundances tend to have lower V_{LSR}, i.e., they lag behind the disk and the high α stars. They also show a larger scatter in their U_{LSR} velocities than the high α stars, see, e.g., Figure 3.28.

We can conclude that this transition region between the halo and the disk needs to be investigated further, with regard to both its abundance and kinematics, and with the help of models.

From the kinematics of the stars, both in our sample, Nissen and Schuster (2010), the Schuster et al. (2006) catalogue and Bensby et al. (in prep.), we found stars which have kinematics similar to two known streams: the Kepley et al. (2007) stream and the Helmi et al. (1999) stream. All the new potential stream stars which are analyzed in our study or in Nissen and Schuster (2010) are part of the low α group of stars. The slope in α-abundances for the low α stars would indicate a slow star formation rate for these stars. This is what one would expect for a smaller galaxy with less gas to form stars from.

We found six new potential members of the Helmi et al. (1999) stream. These stars are all part of the metal-rich population of the Helmi et al. (1999) stream with [Fe/H] ≥ -2.0, compared to the stars in this angular momentum region (Morrison et al., 2009; Roederer et al., 2010).

For the Kepley et al. (2007) stream we found in total 25 new potential members. Twenty of these are from the Schuster et al. (2006) catalogue, and these show a large metallicity spread and an indication of two distinct stellar

populations with different metallicities, Figure 3.20. In a colour-magnitude diagram these two populations do not show any large difference, and from the isoschones we can not clearly say if there is any age differences. However, if we compare the potential stars in the Helmi et al. (1999) stream with the stars in the Kepley et al. (2007) stream we can conclude that the stars in the Helmi et al. (1999) are roughly 2 Gyr younger than the potential stars in the Kepley et al. (2007) stream.

Could this lower age, higher metallicity and more distinct position in angular momentum space be an indication that the Helmi et al. (1999) stream has been accreted later than the Kepley et al. (2007) stream? A higher metallicity of the stream stars would indicate a longer star formation period which could be more likely if the progenitor galaxy were accreted much later in time. Of course this also depends on the type and size of the progenitor galaxy. The question is also if the Kepley et al. (2007) stream is composed by only one or several accreted galaxy, since it occupies a large region in angular momentum space. Further abundance analysis of potential stream stars is needed in order to draw any conclusions regarding which stars would be part of the same stellar stream population. Models might be needed to be able to say if the metallicity span seen for the Helmi et al. (1999) stream can originate from one galaxy and maybe some constrains on this progenitor galaxy can be made. For the the stars in the Kepley et al. (2007) stream more kinematical studies and even models of the stellar obits would be to preferred in order to be able to say if it originated from one accretion event or several.

Bibliography

Arnone, E., Ryan, S. G., Argast, D., Norris, J. E., and Beers, T. C.: 2005, *A&A* **430**, 507

Belokurov, V., Zucker, D. B., Evans, N. W., Gilmore, G., Vidrih, S., Bramich, D. M., Newberg, H. J., Wyse, R. F. G., Irwin, M. J., Fellhauer, M., Hewett, P. C., Walton, N. A., Wilkinson, M. I., Cole, N., Yanny, B., Rockosi, C. M., Beers, T. C., Bell, E. F., Brinkmann, J., Ivezić, Ž., and Lupton, R.: 2006, *ApJ* **642**, L137

Bensby, T., Feltzing, S., and Lundström, I.: 2003, *A&A* **410**, 527

Bensby, T., Feltzing, S., and Lundström, I.: 2004, in A. McWilliam & M. Rauch (ed.), *Origin and Evolution of the Elements*

Bensby, T., Oey, M. S., Feltzing, S., and Gustafsson, B.: 2007, *ApJ* **655**, L89

Cayrel, R., Depagne, E., Spite, M., Hill, V., Spite, F., François, P., Plez, B., Beers, T., Primas, F., Andersen, J., Barbuy, B., Bonifacio, P., Molaro, P., and Nordström, B.: 2004, *A&A* **416**, 1117

Chereul, E., Crézé, M., and Bienaymé, O.: 1999, *A&AS* **135**, 5

Fellhauer, M., Evans, N. W., Belokurov, V., Zucker, D. B., Yanny, B., Wilkinson, M. I., Gilmore, G., Irwin, M. J., Bramich, D. M., Vidrih, S., Hewett, P., and Beers, T.: 2007, *MNRAS* **375**, 1171

Freedman, R. A. and Kaufmann, W. J.: 2005, *Universe*

Gilmore, G., Wyse, R. F. G., and Kuijken, K.: 1989, *ARA&A* **27**, 555

Gnedin, O. Y. and Ostriker, J. P.: 1997, *ApJ* **474**, 223

Gray, D. F.: 2005, *The Observation and Analysis of Stellar Photospheres*

Helmi, A., White, S. D. M., de Zeeuw, P. T., and Zhao, H.: 1999, *Nature* **402**, 53

Hou, L. G., Han, J. L., and Shi, W. B.: 2009, *A&A* **499**, 473

Ivans, I. I., Sneden, C., James, C. R., Preston, G. W., Fulbright, J. P., Höflich, P. A., Carney, B. W., and Wheeler, J. C.: 2003, *ApJ* **592**, 906

Johnston, K. V., Bullock, J. S., Sharma, S., Font, A., Robertson, B. E., and Leitner, S. N.: 2008, *ApJ* **689**, 936

Kepley, A. A., Morrison, H. L., Helmi, A., Kinman, T. D., Van Duyne, J., Martin, J. C., Harding, P., Norris, J. E., and Freeman, K. C.: 2007, *AJ* **134**, 1579

Koch, A., Grebel, E. K., Odenkirchen, M., Martínez-Delgado, D., and Caldwell, J. A. R.: 2004, *AJ* **128**, 2274

Morrison, H. L., Helmi, A., Sun, J., Liu, P., Gu, R., Norris, J. E., Harding, P., Kinman, T. D., Kepley, A. A., Freeman, K. C., Williams, M., and Van Duyne, J.: 2009, *ApJ* **694**, 130

Nissen, P. E. and Schuster, W. J.: 1997, *A&A* **326**, 751

Nissen, P. E. and Schuster, W. J.: 2010, *A&A* **511**, L10+

Odenkirchen, M., Grebel, E. K., Kayser, A., Rix, H., and Dehnen, W.: 2009, *AJ* **137**, 3378

Odenkirchen, M., Grebel, E. K., Rockosi, C. M., Dehnen, W., Ibata, R., Rix, H., Stolte, A., Wolf, C., Anderson, Jr., J. E., Bahcall, N. A., Brinkmann, J., Csabai, I., Hennessy, G., Hindsley, R. B., Ivezić, Ž., Lupton, R. H., Munn, J. A., Pier, J. R., Stoughton, C., and York, D. G.: 2001, *ApJ* **548**, L165

Perryman, M. A. C. and ESA (eds.): 1997, *The HIPPARCOS and TYCHO catalogues. Astrometric and photometric star catalogues derived from the ESA HIPPARCOS Space Astrometry Mission*, Vol. 1200 of *ESA Special Publication*

Roederer, I. U., Sneden, C., Thompson, I. B., Preston, G. W., and Shectman, S. A.: 2010, *ApJ* **711**, 573

Schönrich, R. and Binney, J.: 2009a, *MNRAS* **396**, 203

Schönrich, R. and Binney, J.: 2009b, *MNRAS* **399**, 1145

Schuster, W. J., Moitinho, A., Márquez, A., Parrao, L., and Covarrubias, E.: 2006, *A&A* **445**, 939

Seabroke, G. M., Gilmore, G., Siebert, A., Bienaymé, O., Binney, J., Bland-Hawthorn, J., Campbell, R., Freeman, K. C., Gibson, B., Grebel, E. K., Helmi, A., Munari, U., Navarro, J. F., Parker, Q. A., Siviero, A., Steinmetz, M., Watson, F. G., Wyse, R. F. G., Zwitter, T., Peñarrubia, J., Smith, M. C., and Williams, M.: 2008, *MNRAS* **384**, 11

Wetterer, C. J. and McGraw, J. T.: 1996, *AJ* **112**, 1046

Yanny, B., Newberg, H. J., Johnson, J. A., Lee, Y. S., Beers, T. C., Bizyaev, D., Brewington, H., Fiorentin, P. R., Harding, P., Malanushenko, E., Malanushenko, V., Oravetz, D., Pan, K., Simmons, A., and Snedden, S.: 2009, *ApJ* **700**, 1282

York, D. G., Adelman, J., Anderson, Jr., J. E., Anderson, S. F., Annis, J., Bahcall, N. A., Bakken, J. A., Barkhouser, R., Bastian, S., Berman, E., Boroski, W. N., Bracker, S., Briegel, C., Briggs, J. W., Brinkmann, J., Brunner, R., Burles, S., Carey, L., Carr, M. A., Castander, F. J., Chen, B., Colestock, P. L., Connolly, A. J., Crocker, J. H., Csabai, I., Czarapata, P. C., Davis, J. E., Doi, M., Dombeck, T., Eisenstein, D., Ellman, N., Elms, B. R., Evans, M. L., Fan, X., Federwitz, G. R., Fiscelli, L., Friedman, S., Frieman, J. A., Fukugita, M., Gillespie, B., Gunn, J. E., Gurbani, V. K., de Haas, E., Haldeman, M., Harris, F. H., Hayes, J., Heckman, T. M., Hennessy, G. S., Hindsley, R. B., Holm, S., Holmgren, D. J., Huang, C., Hull, C., Husby, D., Ichikawa, S., Ichikawa, T., Ivezić, Ž., Kent, S., Kim, R. S. J., Kinney, E., Klaene, M., Kleinman, A. N., Kleinman, S., Knapp, G. R., Korienek, J., Kron, R. G., Kunszt, P. Z., Lamb, D. Q., Lee, B., Leger, R. F., Limmongkol, S., Lindenmeyer, C., Long, D. C., Loomis, C., Loveday, J., Lucinio, R., Lupton, R. H., MacKinnon, B., Mannery, E. J., Mantsch, P. M., Margon, B., McGehee, P., McKay, T. A., Meiksin, A., Merelli, A., Monet, D. G., Munn, J. A., Narayanan, V. K., Nash, T., Neilsen, E., Neswold, R., Newberg, H. J., Nichol, R. C., Nicinski, T., Nonino, M., Okada, N., Okamura, S., Ostriker, J. P., Owen, R., Pauls, A. G., Peoples, J., Peterson, R. L., Petravick, D., Pier, J. R., Pope, A., Pordes, R., Prosapio, A., Rechenmacher, R., Quinn, T. R., Richards, G. T., Richmond, M. W., Rivetta, C. H., Rockosi, C. M., Ruthmansdorfer, K., Sandford, D., Schlegel, D. J., Schneider, D. P., Sekiguchi, M., Sergey, G., Shimasaku, K., Siegmund, W. A., Smee, S., Smith, J. A., Snedden,

S., Stone, R., Stoughton, C., Strauss, M. A., Stubbs, C., SubbaRao, M., Szalay, A. S., Szapudi, I., Szokoly, G. P., Thakar, A. R., Tremonti, C., Tucker, D. L., Uomoto, A., Vanden Berk, D., Vogeley, M. S., Waddell, P., Wang, S., Watanabe, M., Weinberg, D. H., Yanny, B., and Yasuda, N.: 2000, *AJ* **120**, 1579

Appendix A

Some additional notes on how to install FIEStool

The installation of FIEStool was trivial. I have two versions of python on my computer, one from scisoft (ESO package of programs) and the one which comes with the Linux installation, which means that I need to tell FIEStool which version I want to use. This is done by first finding out which version is as default.
which python - writes in a terminal
Then the path to the python version will be displayed, this was not the scisoft one which I want FIEStool to use, therefore I needed to change the first line in the FIEStool program **FIEStool.py**
!/usr/bin/env python - where the env python means that the python version used is the default one.
Change this line to - # !/scisoft/bin/python - or to our path to the correct version of python.

After this I tried ./FIEStool.py again, and new error messages occured. First I needed to import _tkinter into python, which is done by starting python (in my case python2.5 for the scisoft version) and writing **import _tkinter**. This is because pyhton was not configured for Tk, which is a graphical environment for python. Python can still work without it but not FIEStool. But before you can do this you may need to disable **SELinux** which is a firewall of some sort which prevents tkinter being loaded. You can find the setting for SELinux under System/Adminitration/Security Level and Firewall.

Then to get **pyraf** to work I needed to have these two lines in **.cshrc** file (which is the file where all the paths are set).
setenv iraf /scisoft/share/iraf/iraf/

setenv IRAFARCH redhat
After this there was also a problem with the **libplot.so.2** file, it could not find the file or directory, therefore also the following path was needed in the same file as before.
setenv LD_LIBRARY_PATH /scisoft/lib/

When you have changed the **.cshrc** file you need to write **source ~/.cshrc** in a terminal to update the changes in the file[1].

After all these adjustments FIEStool started and it looks the way I remember it from the NOT. With only the need to change two pathways inside the FIEStool program files the program worked.

[1]Ross Church helped me with all these additional settings.

Appendix B

Abundances for the 23 analyzed Halo Stars

The following tables, B.1 to B.8, list the abundances, number of lines used for the abundance analysis and σ, for all the elements analyzed in our sample of 23 halo stars.

Table B.1: The Fe abundances for all stars. Column one lists the name of the star. Columns two and five the abundance of Fe I and Fe II. Columns three and six the number of measured lines, and columns four and seven the standard deviation of the abundances of Fe I and Fe II.

Star	[FeI/H]	nr. of lines	σ	[FeII/H]	nr. of lines	σ
HIP3026	-1.14	138	0.15	-1.06	22	0.10
HIP3884	-0.68	163	0.34	-0.83	21	0.29
HIP16404	-2.19	111	0.14	-1.97	11	0.31
HIP22068	-1.46	144	0.13	-1.43	24	0.11
HIP28671	-1.06	178	0.10	-1.04	25	0.14
HIP38541	-1.74	150	0.11	-1.64	20	0.17
HIP42592	-1.98	89	0.17	-1.92	17	0.13
HIP44124	-1.65	95	0.25	-1.58	18	0.32
HIP48152	-2.06	73	0.19	-1.95	18	0.19
HIP51477	-0.98	167	0.12	-0.92	23	0.11
HIP58401	-0.64	162	0.10	-0.63	23	0.29
HIP60632	-1.66	104	0.11	-1.59	18	0.10
HIP62108	-1.58	116	0.14	-1.55	20	0.11
HIP63918	-0.68	181	0.10	-0.52	24	0.09
HIP64920	-0.43	128	0.09	-0.51	24	0.14
HIP65201	-1.70	69	0.14	-1.70	16	0.21
HIP73385	-1.41	143	0.12	-1.38	22	0.13
HIP76976	-2.57	26	0.10	-2.45	7	0.07
HIP78640	-1.43	121	0.12	-1.37	20	0.10
HIP80114	-0.64	183	0.10	-0.61	24	0.06
HIP80837	-0.70	192	0.10	-0.66	26	0.08
HIP86694	-1.75	106	0.11	-1.67	17	0.09
HIP100792	-1.12	156	0.10	-1.04	23	0.08

Table B.2: The Ti abundances for all stars. Column one lists the name of the star. Columns two and five the abundance of Ti I and Ti II. Columns three and six the number of measured lines, and columns four and seven the standard deviation of the abundances of Ti I and Ti II.

Star	[TiI/H]	nr. of lines	σ	[TiII/H]	nr. of lines	σ
HIP3026	-0.92	14	0.13	-0.84	15	0.08
HIP3884	-0.19	25	0.38	-0.38	13	0.43
HIP16404	-1.19	15	0.09	-1.87	11.	0.14
HIP22068	-1.11	21	0.11	-1.17	13	0.10
HIP28671	-0.86	17	0.08	-0.85	15	0.10
HIP38541	-1.51	19	0.10	-1.45	15	0.11
HIP42592	-1.66	11	0.13	-1.72	10	0.21
HIP44124	-1.37	11	0.19	-1.31	10	0.17
HIP48152	-1.59	8	0.09	-1.79	11	0.10
HIP51477	-0.76	21	0.09	-0.63	12	0.07
HIP58401	-0.18	26	0.13	-0.36	13	0.10
HIP60632	-1.32	14	0.09	-1.30	11	0.09
HIP62108	-1.16	14	0.23	-1.09	12	0.23
HIP63918	-0.43	25	0.09	-0.24	13	0.08
HIP64920	-0.09	24	0.11	-0.21	13	0.06
HIP65201	-1.26	8	0.07	-1.48	9	0.14
HIP73385	-1.10	17	0.11	-1.08	16	0.11
HIP76976	-2.34	5	0.22	-2.46	6	0.14
HIP78640	-1.16	15	0.09	-1.11	15	0.09
HIP80114	-0.50	24	0.09	-0.43	12	0.06
HIP80837	-1.48	24	0.09	-0.42	15	0.07
HIP86694	-0.98	12	0.12	-1.51	12	0.10
HIP100792	-0.86	16	0.09	-0.91	15	0.07

Table B.3: The Na and Ni abundances for all stars. Column one lists the name of the star. Columns two and five the abundance of Na and Ni. Columns three and six the number of measured lines, and columns four and seven the standard deviation of the abundances of Na and Ni.

Star	[Na/H]	nr. of lines	σ	[Ni/H]	nr. of lines	σ
HIP3026	-1.37	3	0.12	-1.16	19	0.13
HIP3884	-0.50	4	0.23	-0.50	35	0.36
HIP16404	-2.65	1	0.00	-2.14	11	0.22
HIP22068	-1.44	4	0.08	-1.42	25	0.15
HIP28671	-1.21	4	0.10	-1.18	33	0.12
HIP38541	-1.85	3	0.08	-1.77	24	0.17
HIP42592	-1.90	2	0.04	-1.95	12	0.31
HIP44124	-1.60	1	0.00	-1.52	10	0.37
HIP48152	-2.01	1	0.00	-2.02	6	0.20
HIP51477	-1.07	4	0.14	-0.97	36	0.12
HIP58401	-0.68	4	0.09	-0.62	40	0.11
HIP60632	-1.74	2	0.14	-1.60	12	0.16
HIP62108	-1.66	2	0.06	-1.51	16	0.21
HIP63918	-0.67	4	0.15	-0.63	40	0.10
HIP64920	-0.23	4	0.18	-0.37	41	0.12
HIP65201	-1.89	1	0.00	-1.79	5	0.13
HIP73385	-1.42	4	0.30	-1.31	21	0.14
HIP76976				-2.17	2.00	0.12
HIP78640	-1.44	2	0.08	-1.39	20	0.16
HIP80114	-0.80	4	0.19	-0.68	40	0.10
HIP80837	-0.60	4	0.16	-0.65	43	0.09
HIP86694	-1.43	3	0.16	-1.75	15	0.13
HIP100792	-1.22	4	0.12	-1.15	25	0.12

Table B.4: The Mg and Si abundances for all stars. Column one lists the name of the star. Columns two and five the abundance of Mg and Si. Columns three and six the number of measured lines, and colums four and seven the standard deviation of the abundances of Mg and Si.

Star	[Mg/H]	nr. of lines	σ	[Si/H]	nr. of lines	σ
HIP3026	-1.02	2	0.08	-1.24	15	0.10
HIP3884	-0.38	2	0.18	-0.63	13	0.21
HIP16404	-1.96	2	0.08	-	-	-
HIP22068	-1.15	2	0.14	-1.18	15	0.06
HIP28671	-0.94	2	0.18	-0.99	16	0.04
HIP38541	-1.46	2	0.06	-1.54	11	0.16
HIP42592	-1.76	2	0.02	-1.74	10	0.21
HIP44124	-1.39	2	0.13	-1.40	7	0.14
HIP48152	-1.86	2	0.26	-1.84	5	0.20
HIP51477	-0.66	2	0.06	-0.66	15	0.05
HIP58401	-0.54	2	0.07	-1.35	16	0.09
HIP60632	-1.35	2	0.12	-1.35	11	0.13
HIP62108	-1.33	2	0.05	-1.33	15	0.09
HIP63918	-0.40	2	0.03	-0.42	11	0.05
HIP64920	-0.10	2	0.00	-0.22	16	0.09
HIP65201	-1.50	2	0.10	-1.62	3	0.10
HIP73385	-1.01	2	0.04	-1.03	13	0.08
HIP76976	-2.38	1	0.00	-	-	-
HIP78640	-1.10	2	0.11	-1.13	14	0.06
HIP80114	-0.50	2	0.08	-0.55	16	0.06
HIP80837	-0.41	2	0.07	-0.50	17	0.05
HIP86694	-1.61	2	0.17	-1.51	12	0.09
HIP100792	-0.95	2	0.10	-0.97	15	0.10

Table B.5: The Ca abundances for all stars. Column one lists the name of the star. Columns two the abundance of Ca. Columns three the number of measured lines, and columns four the standard deviation of the abundances of Ca and CrI.

Star	[Ca/H]	nr. of lines	σ
HIP3026	-0.79	16	0.09
HIP3884	-0.39	15	0.40
HIP16404	-1.87	13	0.14
HIP22068	-1.07	17	0.14
HIP28671	-0.75	18	0.08
HIP38541	-1.41	19	0.08
HIP42592	-1.57	16	0.11
HIP44124	-1.38	13	0.10
HIP48152	-1.62	14	0.12
HIP51477	-0.65	18	0.07
HIP58401	-0.43	18	0.14
HIP60632	-1.25	17	0.09
HIP62108	-1.13	17	0.09
HIP63918	-0.41	18	0.05
HIP64920	-0.14	18	0.06
HIP65201	-1.28	12	0.10
HIP73385	-1.04	15	0.10
HIP76976	-2.15	9	0.14
HIP78640	-1.01	15	0.10
HIP80114	-0.46	18	0.06
HIP80837	-0.44	17	0.08
HIP86694	-1.36	16	0.10
HIP100792	-0.85	16	0.08

Table B.6: The CrI and CrII abundances for all stars. Column one lists the name of the star. Columns two and five the abundance of CrI and CrII. Columns three and six the number of measured lines, and columns four and seven the standard deviation of the abundances of CrI and CrII.

Star	[CrI/H]	nr. of lines	σ	[CrII/H]	nr. of lines	σ
HIP3026	-1.06	5	0.15	-1.09	7	0.11
HIP3884	-0.42	9	0.28	-0.54	8	0.60
HIP16404	-2.1	3	0.05	-2.01	2	0.05
HIP22068	-1.39	5	0.10	-1.43	4	0.13
HIP28671	-0.99	8	0.08	-1.03	7	0.12
HIP38541	-1.59	4	0.10	-1.74	4	0.10
HIP42592	-1.79	2	0.16	-1.99	3	0.16
HIP44124	-1.55	3	0.13	-1.55	3	0.09
HIP48152	-2.16	2	0.04	-2.17	3	0.28
HIP51477	-0.96	7	0.04	-0.95	4	0.14
HIP58401	-0.55	10	0.09	-0.61	4	0.08
HIP60632	-1.58	4	0.19	-1.61	3	0.06
HIP62108	-1.26	4	0.27	-1.6	3	0.22
HIP63918	-0.65	8	0.05	-0.53	4	0.15
HIP64920	-0.42	11	0.15	-0.50	4	0.09
HIP65201	-1.57	1	-	-1.79	2	0.02
HIP73385	-1.24	5	0.21	-1.39	6	0.12
HIP76976	-	-	-	-2.38	3	0.32
HIP78640	-1.34	5	0.18	-1.44	6	0.10
HIP80114	-0.62	9	0.05	-0.64	4	0.14
HIP80837	-0.60	8	0.13	-0.70	8	0.12
HIP86694	-1.86	3	0.07	-1.64	4	0.16
HIP100792	-1	5	0.16	-1.09	7	0.10

Table B.7: The YII and BaII abundances for all stars. Column one lists the name of the star. Columns two and five the abundance of YII and BaII. Columns three and six the number of measured lines, and colums four and seven the standard deviation of the abundances of YII and BaII.

Star	[YII/H]	nr. of lines	σ	[BaII/H]	nr. of lines	σ
HIP3026	-1.95	6	0.14	-1.00	4	0.22
HIP3884	-0.22	6	0.49	-0.91	3	0.21
HIP16404	-2.41	3	0.13	-2.43	3	0.16
HIP22068	-1.52	6	0.14	-1.27	4	0.33
HIP28671	-1.17	5	0.07	-0.86	3	0.14
HIP38541	-1.81	6	0.17	-1.82	3	0.09
HIP42592	-1.96	6	0.15	-1.79	4	0.34
HIP44124	-1.71	5	0.15	-1.81	4	0.10
HIP48152	-2.04	4	0.23	-2.27	4	0.08
HIP51477	-0.74	6	0.12	-0.52	4	0.08
HIP58401	-0.55	6	0.10	-0.64	4	0.05
HIP60632	-1.71	6	0.13	-1.61	4	0.25
HIP62108	-1.43	6	0.12	-1.47	4	0.19
HIP63918	-0.52	6	0.12	-0.45	4	0.09
HIP64920	-0.38	6	0.17	-0.39	4	0.12
HIP65201	-1.82	4	0.16	-1.68	4	0.2
HIP73385	-1.23	6	0.16	-1.18	3	0.19
HIP76976	-	-	-	-3.59	2	0.13
HIP78640	-1.38	6	0.14	-1.42	4	0.23
HIP80114	-0.72	6	0.10	-0.50	4	0.04
HIP80837	-0.83	6	0.10	-0.62	3	0.17
HIP86694	-1.86	6	0.15	-1.41	4	0.33
HIP100792	-1.22	6	0.10	-1.02	3	0.19

Table B.8: The Al and Zn abundances for all stars. Column one lists the name of the star. Columns two and five the abundance of Al and Zn. Columns three and six the number of measured lines, and colums four and seven the standard deviation of the abundances of Al and Zn.

Star	[Al/H]	nr. of lines	σ	[Zn/H]	nr. of lines	σ
HIP3026	-	-	-	-1.01	3	0.16
HIP3884	-0.33	3	0.07	-0.83	2	0.11
HIP16404	-	-	-	-1.87	2	0.06
HIP22068	-	-	-	-1.32	2	0.05
HIP28671	-1.05	1	0	-0.93	3	0.11
HIP38541	-	-	-	-1.57	2	0.04
HIP42592	-	-	-	-1.70	2	0.02
HIP44124	-	-	-	-1.65	2	0.09
HIP48152	-	-	-	-1.79	2	0.01
HIP51477	-0.85	1	0	-0.7	3	0.05
HIP58401	-0.31	3	0.18	-0.60	3	0.05
HIP60632	-	-	-	-1.46	2	0.07
HIP62108	-	-	-	-1.39	3	0.06
HIP63918	-0.43	3	0.07	-0.36	3	0.03
HIP64920	-0.02	3	0.22	-0.15	3	0.15
HIP65201	-	-	-	-1.65	1	-
HIP73385	-	-	-	-1.2	2	0.04
HIP76976	-	-	-	-2.3	2	0.16
HIP78640	-	-	-	-1.24	2	0.02
HIP80114	-0.51	2	0-06	-0.51	3	0.01
HIP80837	-0-57	0	0	-0.42	3	0.12
HIP86694	-	-	-	-1.62	2	0.11
HIP100792	-	-	-	-0.95	3	0.16